CSIAM Trans. Appl. Math.
doi: 10.4208/csiam-am.SO-2022-0019

Vol. **4**, No. 1, pp. 177-224
March 2023

Unconditionally Maximum-Principle-Preserving Parametric Integrating Factor Two-Step Runge-Kutta Schemes for Parabolic Sine-Gordon Equations

Hong Zhang[1,*], Xu Qian[1], Jun Xia[2] and Songhe Song[1]

[1] *Department of Mathematics, National University of Defense Technology, Changsha 410073, China.*
[2] *College of Basic Education, National University of Defense Technology, Changsha, Hunan 410073, China.*

Received 26 May 2022; Accepted 8 October 2022

Abstract. We present a systematic two-step approach to derive temporal up to the eighth-order, unconditionally maximum-principle-preserving schemes for a semilinear parabolic sine-Gordon equation and its conservative modification. By introducing a stabilization term to an explicit integrating factor approach, and designing suitable approximations to the exponential functions, we propose a unified parametric two-step Runge-Kutta framework to conserve the linear invariant of the original system. To preserve the maximum principle unconditionally, we develop parametric integrating factor two-step Runge-Kutta schemes by enforcing the non-negativeness of the Butcher coefficients and non-decreasing constraint of the abscissas. The order conditions, linear stability, and convergence in the L^∞-norm are analyzed. Theoretical and numerical results demonstrate that the proposed framework, which is explicit and free of limiters, cut-off post-processing, or exponential effects, offers a concise, and effective approach to develop high-order inequality-preserving and linear-invariant-conserving algorithms.

AMS subject classifications: 65L06, 65M12, 35B50, 35K55

Key words: Parabolic sine-Gordon equation, linear-invariant-conserving, unconditionally maximum-principle-preserving, parametric two-step Runge-Kutta method.

1 Introduction

Many differential equations in fluid dynamics, physics, chemistry, biology, engineering, and material science are naturally equipped with inequality constraints on the solution

*Corresponding author. *Email addresses:* zhanghnudt@163.com (H. Zhang), qianxu@nudt.edu.cn (X. Qian), 68475460@qq.com (J. Xia), shsong@nudt.edu.cn (S. Song)

components, such as strong stability [30], positivity [78], maximum principle [19,54], and contractivity [48] constraints. It is recognized that preserving these inequality structures is not only important for solutions to be physically meaningful but also relevant for the numerical stability of time integration methods. In the last three decades, the development of high-order accurate and efficient algorithms that can preserve such inequalities has been a serious research objective [10,36,39,40,55,66]. However, it still remains an outstanding open problem [3] to develop numerical methods that are both (i) of high-order accuracy and (ii) capable of preserving inequality structures for any time-step size. To the best of our knowledge, the high-order methods that can unconditionally guarantee these properties are very limited [4, 19, 28, 46]. This motivated us to pursue high-order-accurate and stable explicit schemes that can preserve the above inequality structures for any time step. In particular, we selected the preservation of the maximum principle for newly developed semilinear parabolic sine-Gordon equations as an example.

Recently, starting from the semilinear parabolic Allen-Cahn (AC) equation [1] and hyperbolic sine-Gordon equation [23], Cheng *et al.* [11] proposed and analyzed a parabolic sine-Gordon (pSG) equation. They rigorously analyzed the existence of a maximum principle, bounded steady states, a conditionally maximum-principle-preserving (MPP) first-order implicit-explicit (IMEX) scheme, and an energy-stable second-order backward differentiation formula (BDF2) scheme. The pSG equation is interesting for a number of reasons. First and foremost, Cheng *et al.* [11] demonstrated that the pSG model exhibits striking similarity with the classical AC equation (Ginzburg-Landau potential). Because of its very benign nonlinear structure, one can develop unconditionally MPP schemes. Thus, it is of purely mathematical interest as a suitable testbed for phase field simulations, and is expected to have a ubiquitous presence [11]. Moreover, from a physical perspective, the pSG equation (with a white noise term and suitable parameters) is closely related to models of a globally neutral gas of interacting charges [31], most directly it is the natural (Langevin) dynamics for the sine-Gordon (Euclidean) quantum filed theory [7]. Hairer and Shen [31] showed that the pSG equation with white noise also arises naturally from a class of equilibrium interface fluctuation models with periodic nonlinearities. In addition, it was also proposed as a model for the dynamics of crystal-vapour interfaces at the roughening transition [56], and has attracted much attention [32] in recent years. Therefore, the development of efficient and stable schemes for the pSG equation has practical significance. Consider the semilinear pSG equation [11]

$$\begin{cases} u_t = \epsilon^2 \Delta u + f(u), & x \in \Omega, \quad t \in (0,T], \\ u(x,0) = u^0(x), & x \in \bar{\Omega}, \end{cases} \tag{1.1}$$

where the unknown function u represents the difference between the concentrations of the two components, $\Omega \in \mathbb{R}^d$ is an open, connected, and bounded region with a Lipschitz boundary $\partial\Omega$, and periodic or homogeneous Neumann boundary conditions. The nonlinear function $f(u) = \sin(u)$ is the negative derivative of a cosine potential function $F(u) = \cos(u)$.

Note that the pSG equation does not conserve the phase variable, that is to say, the total amount of the two components (e.g., gas and plasma when modeling a globally neutral gas of interacting charges [31]) will change during the evolutions. To carry out simulations that conserve the mass, we study the conservative pSG equation

$$u_t = \epsilon^2 \Delta u + \bar{f}(u), \tag{1.2}$$

following the work of Li *et al.* [52] where a Rubinstein-Sternberg-type Lagrangian multiplier [58] was introduced to the AC equation. The modified nonlinear term in (1.2) is defined as $\bar{f}(u) := f(u) - \lambda(t)$, with $\lambda(t)$ being the non-local Lagrange multiplier proposed by Rubinstein and Sternberg [58],

$$\text{RSLM:} \quad \lambda(t) = \frac{1}{|\Omega|} \int_\Omega f(u) \mathrm{d}x, \tag{1.3}$$

to enforce the conservation of mass $M(u) = (u,1)$,

$$\frac{\mathrm{d}M(u)}{\mathrm{d}t} = 0, \ \ \forall t > 0, \tag{1.4}$$

under periodic or homogeneous Neumann boundary conditions. The symbol $(\cdot,\cdot)$, which denotes the standard L^2 inner product, is defined as $(u,v) = \int_\Omega uv \mathrm{d}x$. We denote the modification (1.2) with the Lagrange multiplier (1.3) as the RSLM formulation.

Cheng *et al.* [11] proved that the parabolic equation (1.1) with a cosine potential function admits a maximum principle, i.e., if the supremum norms of the initial and boundary conditions are bounded by $\beta = \pi$, then the solution will always satisfy $\|u(x,t)\|_{L^\infty} \le \beta$, $\forall t > 0$. In addition to the maximum principle, another intrinsic property of the pSG equation is the dissipation of energy, i.e.,

$$\frac{\mathrm{d}}{\mathrm{d}t} E(u) = -\int_\Omega \left| \frac{\partial u}{\partial t} \right|^2 \mathrm{d}x \le 0, \quad \forall t > 0$$

with the energy functional given by

$$E(u) = \int_\Omega \frac{1}{2} \epsilon^2 |\nabla u|^2 + \cos(u) \, \mathrm{d}x. \tag{1.5}$$

It is known that the introduction of the RSLM formulation in the classical AC equation changes the maximum principle of the original equation, but retains the energy dissipation law [58]. As is shown in [44, 52, 57], it is of great importance to develop schemes to preserve the structures of conservative AC-type equations, i.e., the preservation of the maximum principle, conservation of mass, and dissipation of energy. Otherwise, the numerical solution may be unstable, and the properties of the original equations will be destroyed. In the literature, semilinear parabolic equations in the form of (1.1) with the Ginzburg-Landau polynomial potential function

$$F(u) = \frac{1}{4}(u^2 - 1)^2$$

or the Flory-Huggins logarithmic potential function

$$F(u)=\frac{\theta}{2}\big[(1+u)\ln(1+u)+(1-u)\ln(1-u)\big]-\frac{\theta_c}{2}u^2$$

have been widely investigated [18,19,33,61,65]. Still, further studies on the pSG equation and its RSLM formulation are lacking.

Parabolic equations are difficult to solve because of their strong stiffness. The stiffness of such equations comes from high-order spatial derivatives. When a stiff partial differential equation is to be solved by a general explicit scheme, the stability usually forces the time step to be much smaller than that imposed by the accuracy. Although implicit schemes can overcome this limitation, for many practical problems, a fully implicit treatment may be structurally difficult or computationally costly. As a compromise between efficiency and stability at large time steps, the development of high-order-accurate and stable linearly implicit/explicit schemes for stiff equations has received much attention in recent years [6,8,18,24,45,60,73].

As demonstrated by Du *et al.* [19], as well as in earlier papers [15, 22, 34, 61, 62, 69], a concise and effective technique for improving the stability of a numerical method is to add and subtract a linear term to and from the original system. Such linearly stabilized schemes have been widely used to construct unconditionally MPP and energy stable schemes. Tang and Yang [65] proposed the first unconditionally MPP scheme, in which the first-order IMEX Euler scheme was combined with a stabilization technique. Using the energy factorization together with a stabilization approach, Wang *et al.* [67,68] developed first-order semi-implicit schemes with small stabilization parameters to preserve the maximum principle unconditionally. However, traditional high-order temporal integrators fail to preserve the maximum principle because of the lack of strategies for dealing with the stiff term and stabilization term. By utilizing exponential time difference (ETD) methods and a stabilization technique, Du *et al.* [18] developed two unconditionally MPP schemes for a non-local AC equation equipped a non-local operator, i.e., the first-order ETD1 scheme and the second-order ETD2 scheme. The ETD schemes have become popular in recent years. Du *et al.* [19] further proved that ETD schemes can preserve the maximum principle unconditionally for a class of semilinear parabolic equations. Li *et al.* [52] and Jiang *et al.* [44] showed these ETD schemes not only preserve the maximum principle unconditionally but also conserve the mass when applied to conservative AC equations. Very recently, Ju *et al.* [45] proved that the ETD schemes incorporated with generalized scalar auxiliary variables unconditionally preserve the maximum principle and are stable with respect to a modified energy.

The stabilization technique has also been introduced to the integrating factor Runge-Kutta (IFRK) framework. To eliminate the exponential decay or growth in the integrating factor approach, some novel strategies have been developed. Starting from the traditional integrating factor RK and multi-step schemes, Huang and Shu [38] first proposed replacing the exponential functions with polynomial functions without destroying the convergence, hence obtaining high-order modified exponential RK and multi-step meth-

ods that can preserve the bounds for scalar hyperbolic equations with stiff source terms. Du *et al.* [16, 17] proposed second- and third-order modified exponential RK schemes by using conservative approximations that were combinations of linear and exponential functions. Recently, a recurrent approximation that bypasses some typical challenges, such as exponential effects and stability issues, was introduced by Zhang *et al.* [77] to develop unconditionally MPP and mass-conserving parametric IFRK (pIFRK) schemes up to the fourth-order. The above approaches simplify the design of explicit, high-order accurate, stable schemes and are applicable to a wide range of applications [63, 72].

The objective of this work is to derive efficient, high-order-accurate, and stable inequality-preserving schemes. Although the focus of this work is mainly on the maximum principle and mass conservation of pSG equations, the proposed integrators can be applied to preserve other inequality structures without any difficulty. To achieve this goal, we investigate the approximations of combining exponential and linear functions in the integrating factor (IF) two-step Runge-Kutta (TSRK) framework and propose a new recurrent approximation incorporating Taylor expansions. When considering the preservation of the maximum principle, it is important to construct a spatial discretization that inherits the maximum principle. In the literature, the central finite difference (FD) method plays a key role in constructing MPP schemes [18, 53, 71, 76], because of its diagonally dominant property. Another popularly used spatial discretization method for semilinear parabolic equations is the Fourier pseudo-spectral (FP) discretization [9, 21, 26, 35]. However, high-order spatial discretizations in general do not inherit the maximum principle [71]. Therefore, it is also meaningful to explore the performance of high-order MPP temporal integrators combined with high-order spatial discretizations. Compared with the existing literature, the novel contributions of this work include the following:

- A new strategy to construct high-order stabilization schemes for stiff nonlinear problems is proposed by adopting the integrating factor two-step Runge-Kutta method.

- Two novel approximations are developed in a unified framework to eliminate exponential decay/growth effects of integrating-factor two-step Runge-Kutta (IFTSRK) schemes, which result in two types of linear-invariant-conserving parametric TSRK (pTSRK) schemes up to the eighth-order.

- By incorporating an integrating factor $e^{-t\mathcal{L}}$, under suitable requirements of the stabilization parameter, we derive sufficient conditions for the parametric IFTSRK (pIFTSRK) schemes to be unconditionally MPP, i.e., the coefficients are non-negative, and the abscissas are non-decreasing.

- The proposed parametric schemes are explicit, free of limiters or cut-off post-processing. In addition, they can unconditionally preserve many inequality structures characterized by forward Euler conditions, such as strong stability, positivity, and contractivity.

The rest of this paper is organized as follows. Section 2 presents some preliminaries for the model equations. In Section 3, we start with a linear-invariant-conserving improvement over the traditional integrating factor approach and illustrate the main ideas to construct up to the eighth-order unconditionally inequality-preserving schemes. The linear stability analysis and error estimates are analyzed in Section 4. In Section 5, various experiments are considered to demonstrate the effectiveness and advantages of proposed schemes. Some concluding remarks are presented in Section 6.

2 Preliminaries

The pSG equation and its conservative RSLM formulation belong to a family of semilinear parabolic equations with the form

$$u_t = \mathcal{L}u + \mathcal{N}(u). \tag{2.1}$$

Du *et al.* [19] investigated sufficient conditions for the abstract framework (2.1) to have a maximum principle:

1. The linear operator $\mathcal{L}$ is dissipative in the sense that if a function w reaches its maximum on $\bar{\Omega}=\Omega\cup\partial\Omega$ at $x_0\in\Omega$, then it must hold that $\mathcal{L}w(x_0)\leq 0$.
2. There exist a $\beta>0$ and a $\kappa>0$, such that the nonlinear term $\mathcal{N}(u)$ satisfies the inequality
$$\|N(u)+\kappa u\|_{L^\infty}\leq\kappa\beta,\quad \forall\|u\|_{L^\infty}\leq\beta. \tag{2.2}$$

Here, the inequality (2.2) is denoted as a circle condition (which also appeared in [29,48]), which means that $\mathcal{N}(u)$ is bounded by a 'circle' measured by $\|\cdot\|_{L^\infty}$ that is centered at $-\kappa u$ with a radius $\kappa\beta$. Noting that the Laplacian satisfies the first condition, we have following lemmas.

Lemma 2.1 ([19])**.** *The linear operator $\mathcal{L}:=\epsilon^2\Delta$ with periodic or homogeneous Neumann boundary conditions generates a contraction semi-group $\{S_{\mathcal{L}}(t)=\mathrm{e}^{t\mathcal{L}}\}_{t\geq 0}$ with respect to the infinity norm $\|\cdot\|_{L^\infty}$ on the subspace of $C(\bar{\Omega})$. Moreover, for $\kappa\geq 0$, let $\mathcal{L}_\kappa:=\mathcal{L}-\kappa$. It holds that*

$$\|\mathrm{e}^{t\mathcal{L}_\kappa}u\|_{L^\infty}\leq\mathrm{e}^{-\kappa t}\|u\|_{L^\infty},\quad \forall t>0,\quad u\in C^2(\bar{\Omega}). \tag{2.3}$$

Lemma 2.2. *Under periodic or homogeneous Neumann boundary conditions, it holds that*

$$(\mathrm{e}^{t\mathcal{L}}u,1)=(u,1),\quad \forall t>0,\quad u\in C^2(\bar{\Omega}). \tag{2.4}$$

Proof. Noting that $v(t)=\mathrm{e}^{t\mathcal{L}}u$ is the analytical solution to

$$\begin{cases} v_t=\mathcal{L}v, & t\in(0,T],\\ v(0)=u, \end{cases} \tag{2.5}$$

and Eq. (2.5) is mass conservative under periodic or homogeneous Neumann boundary conditions, it holds that $(v(t),1)=(\mathrm{e}^{t\mathcal{L}}u,1)=(u,1)$. □

For the pSG equation with $\mathcal{N}(u):=f(u)$, for any $\beta\in[(2n-1)\pi,2n\pi]$,$n\in\mathbb{Z}^+$, when $\|u\|_{L^\infty}\leq\beta$ and $\kappa\geq\max_{|\xi|\leq\beta}|f'(\xi)|=1$, the circle condition is satisfied

$$-\kappa\beta\leq f(-\beta)-\kappa\beta\leq f\big(u(x)\big)+\kappa u(x)\leq f(\beta)+\kappa\beta\leq\kappa\beta,\quad \text{a.e.}\quad x\in\bar{\Omega}.$$

For the conservative RSLM formulation (1.2), the following result holds.

Lemma 2.3. *Let*

$$\beta=\left(2n-\frac{1}{2}\right)\pi,\quad n\in\mathbb{Z}^+\quad \textit{and}\quad \kappa\geq\max_{|\xi|\leq\beta}|f'(\xi)|=1.$$

The nonlinear function

$$\mathcal{N}(u):=f(u)-\frac{1}{|\Omega|}\int_\Omega f(u)\,\mathrm{d}x$$

satisfies the circle condition (2.2).

Proof. Noting that

$$\|f(u)\|_{L^\infty}\leq f(-\beta)=-f(\beta)=1,$$

we obtain

$$f(\beta)\leq\frac{1}{|\Omega|}\int_\Omega f(u)\mathrm{d}x\leq f(-\beta).$$

When $\kappa\geq\max_{|\xi|\leq\beta}|f'(\xi)|$ and $\|u\|_{L^\infty}\leq\beta$, we obtain

$$f(-\beta)-\kappa\beta\leq f\big(u(x)\big)+\kappa u(x)\leq f(\beta)+\kappa\beta,\quad \text{a.e.}\quad x\in\bar{\Omega}.$$

Then, it holds that

$$\begin{aligned}-\kappa\beta\leq f(-\beta)-\kappa\beta-\frac{1}{|\Omega|}\int_\Omega f\big(u(x)\big)\mathrm{d}x\leq\mathcal{N}\big(u(x)\big)+\kappa u(x)\\ \leq f(\beta)+\kappa\beta-\frac{1}{|\Omega|}\int_\Omega f\big(u(x)\big)\mathrm{d}x\leq\kappa\beta,\quad \text{a.e.}\quad x\in\bar{\Omega}.\end{aligned}$$

This completes the proof. □

By applying previous results in [19,52], we have the following lemma.

Lemma 2.4. *For the semilinear parabolic equation* (2.1), *suppose that*

$$\text{pSG/RSLM}:\quad \kappa\geq\max_{|\xi|\leq\beta}|f'(\xi)|=1. \tag{2.6}$$

Let $\mathcal{N}_\kappa(u)=\mathcal{N}(u)+\kappa u$, *where* $\mathcal{N}(u)$ *is given by* $f(u)$ *for the* pSG *equation and* $\bar{f}(u)$ *for the* RSLM *formulation, respectively. It holds that*

1) $\|\mathcal{N}_\kappa(u)\|_{L^\infty}\leq\kappa\beta$ *for any* $u(x)\in L^\infty(\Omega)$ *with* $\|u\|_{L^\infty}\leq\beta$,

2) $\|\mathcal{N}_\kappa(u_1)-\mathcal{N}_\kappa(u_2)\|_{L^\infty}\le l\kappa\|u_1-u_2\|_{L^\infty}$ *for any* $u_j(x)\in L^\infty(\Omega)$ *with* $\|u_j\|_{L^\infty}\le\beta$, $j=1,2$,

where $\beta\in[(2n-1)\pi,2n\pi]$, $n\in\mathbb{Z}^+$, $l=2$ *for the* pSG *equation, and* $\beta=(2n-1/2)\pi$, $n\in\mathbb{Z}^+$, $l=3$ *for the corresponding* RSLM *formulation.*

By applying Lemmas 2.1 and 2.4 and the abstract framework proposed by Du *et al.* [19], we present the maximum principles for the pSG and RSLM formulations.

Theorem 2.1. *For the* pSG *equation* (1.1) *and the* RSLM *formulation* (1.2) *with either periodic, or homogeneous Neumann boundary conditions, supposing* $u^0\in X$, *where* X *is* $L^\infty(\Omega)$ *or* $C(\bar{\Omega})$, *then each problem has a unique solution* $u\in C([0,T];X)$ *and admits the maximum principle*

$$\begin{aligned}
\text{pSG:}\quad & \forall\beta\in[(2n-1)\pi,2n\pi],\quad n\in\mathbb{Z}^+,\quad \textit{it holds that}\\
& \|u(t)\|_{L^\infty}\le\beta,\quad \forall\|u^0\|_{L^\infty}\le\beta,\quad \forall t\in[0,T],\\
\text{RSLM:}\quad & \forall\beta=\left(2n-\frac{1}{2}\right)\pi,\quad n\in\mathbb{Z}^+,\quad \textit{it holds that}\\
& \|u(t)\|_{L^\infty}\le\beta,\quad \forall\|u^0\|_{L^\infty}\le\beta,\quad \forall t\in[0,T].
\end{aligned}$$

3 Structure-preserving discretizations

To construct efficient time integrators for general stiff, nonlinear differential equations, three key design principles [2, 6, 12, 17] have been considered previously:

1) Linear invariants of the system are preserved.

2) The nonlinear term is handled simply and inexpensively.

3) The time-step size is selected to reflect the accuracy requirement rather than being restricted by a stability requirement.

It is acknowledged that the more principles a numerical method can fulfill, the better its applicability is. In this section, we investigate modifications of the integrating factor approach and construct new parametric methods in which above principles are achieved. To present the schemes in a unified framework and avoid the excessive introduction of symbols, we remark that some symbols, for example, $\psi_i(\tau\kappa)$, $\hat{a}_{i,j}(\tau\kappa)$ and $\hat{d}_{i,j}(\tau\kappa)$, have different definitions in different modifications.

3.1 First parametric two-step Runge-Kutta method

By introducing a stabilization term $\kappa(u-u),\kappa>0$ to the abstract system (2.1), we consider the system

$$\begin{cases} u_t=\mathcal{L}u+\mathcal{N}(u)+\kappa u-\kappa u,\\ u(0)=u^0 \end{cases} \tag{3.1}$$

with periodic or Neumann boundary conditions. When Eq. (3.1) is given by the RSLM formulation (1.2), it holds that

$$(\mathcal{L}u+\mathcal{N}(u),1)=(\epsilon^2\Delta u,1)+\int_\Omega\left[f(u)-\frac{1}{|\Omega|}\int_\Omega f(u)\mathrm{d}x\right]\mathrm{d}x\equiv 0.$$

Then, it is expected that a numerical method will conserve the mass $M(u)$.

To better illustrate the construction of the proposed framework, we first treat both the linear and nonlinear terms explicitly, although the stiff linear term could lead to severe time-step restriction for the fully discrete system. Consider an s-stage, p-th order explicit TSRK(s,p) scheme that does not rely on the stage values of the previous steps, as presented in the form of a Butcher-like tableau

$$\begin{array}{c|c|c}c & D & A\\ \hline c_s & \theta^T & b^T\end{array}=\begin{array}{c|cc|ccccc}c_{-1} & 1 & 0 & 0 & & & & \\ c_0 & 0 & 1 & 0 & 0 & & & \\ c_1 & d_{1,-1} & d_{1,0} & a_{1,-1} & a_{1,0} & 0 & & \\ \vdots & \vdots & \vdots & \vdots & \vdots & \ddots & \ddots & \\ c_{s-1} & d_{s-1,-1} & d_{s-1,0} & a_{s-1,-1} & a_{s-1,0} & a_{s-1,1} & \cdots & 0\\ \hline c_s & d_{s,-1} & d_{s,0} & a_{s,-1} & a_{s,0} & a_{s,1} & \cdots & a_{s,s-1}\end{array}, \tag{3.2}$$

where

$$a_{i,j}=0,\quad i\le j,\quad \sum_{j=-1}^{0}d_{i,j}=1,\quad c_i=-d_{i,-1}+\sum_{j=-1}^{i-1}a_{i,j},\quad i=-1,0,\ldots,s,$$

and coefficients are constrained by certain accuracy and stability requirements [40,42,43,47]. Considering the Lawson transformation [49], with $\mathrm{e}^{t\kappa}$ being the integrating factor to the unknown $u(t)$, i.e., $v(t)=\mathrm{e}^{\kappa t}u(t)$, we obtain an equivalent system

$$\begin{cases}v_t=\mathrm{e}^{\kappa t}\left[\mathcal{L}\mathrm{e}^{-\kappa t}v+\mathcal{N}(\mathrm{e}^{-\kappa t}v)+\kappa\mathrm{e}^{-\kappa t}v\right],\quad t\in(0,T],\\ v(0)=u^0.\end{cases} \tag{3.3}$$

Letting $c_{-1}=-1$, $c_0=0$, and $u^{n+j}=u(t_n+c_j\tau)$, $j=-1,0$, we apply the TSRK method to Eq. (3.3) and then perform the inverse Lawson transformation to obtain the IFTSRK method

$$\begin{cases}u_{n,j}=u^{n+j},\quad j=-1,0, & \text{(3.4a)}\\ u_{n,i}=\displaystyle\sum_{j=-1}^{0}d_{i,j}\mathrm{e}^{-(c_i-c_j)\tau\kappa}u_{n,j}\\ \qquad\quad +\tau\displaystyle\sum_{j=-1}^{i-1}a_{i,j}\mathrm{e}^{-(c_i-c_j)\tau\kappa}\left[\mathcal{L}u_{n,j}+\mathcal{N}(u_{n,j})+\kappa u_{n,j}\right],\quad i=1,\ldots,s, & \text{(3.4b)}\\ u^{n+1}=u_{n,s}. & \text{(3.4c)}\end{cases}$$

Assuming that

$$M(u_{n,j})=(u_{n,j},1)=(u^0,1),\quad j=-1,0,\ldots,i-1,$$

taking the L^2 inner product on both sides of (3.4) with 1, and using the equality

$$\big(\mathcal{L}u_{n,j}+\mathcal{N}(u_{n,j}),1\big)=0,$$

we obtain

$$\begin{aligned}(u_{n,i},1)&=\sum_{j=-1}^{0}d_{i,j}\mathrm{e}^{-(c_i-c_j)\tau\kappa}(u_{n,j},1)+\tau\sum_{j=-1}^{i-1}a_{i,j}\mathrm{e}^{-(c_i-c_j)\tau\kappa}\Big[\underbrace{\big(\mathcal{L}u_{n,j}+\mathcal{N}(u_{n,j}),1\big)}_{=0}+\kappa(u_{n,j},1)\Big]\\&=\mathrm{e}^{-(1+c_i)\tau\kappa}\left[\sum_{j=-1}^{0}d_{i,j}\mathrm{e}^{(1+c_j)\tau\kappa}+\tau\kappa\sum_{j=-1}^{i-1}a_{i,j}\mathrm{e}^{(1+c_j)\tau\kappa}\right](u^0,1),\quad i\le s.\end{aligned}\tag{3.5}$$

Note that $\mathrm{e}^{(1+c_i)\tau\kappa}$ in general is not equal to $[\sum_{j=-1}^{0}d_{i,j}\mathrm{e}^{(1+c_j)\tau\kappa}+\tau\kappa\sum_{j=-1}^{i-1}a_{i,j}\mathrm{e}^{(1+c_j)\tau\kappa}]$ unless $\tau\kappa=0$. Therefore, IFTSRK is not conservative unless the initial mass $(u^0,1)$ equals zero. To overcome this shortcoming, we propose an approximation of $\mathrm{e}^{(1+c_i)\tau\kappa}$ using

$$\psi_i(\tau\kappa):=\sum_{j=-1}^{0}d_{i,j}\mathrm{e}^{(1+c_j)\tau\kappa}+\tau\kappa\sum_{j=-1}^{i-1}a_{i,j}\mathrm{e}^{(1+c_j)\tau\kappa},\quad i=-1,\ldots,s.\tag{3.6}$$

Then, stage solutions of (3.4) are given by

$$\begin{aligned}&u_{n,i}=\frac{1}{\psi_i(\tau\kappa)}\left(\sum_{j=-1}^{0}d_{i,j}\mathrm{e}^{(1+c_j)\tau\kappa}u_{n,j}+\tau\sum_{j=-1}^{i-1}a_{i,j}\mathrm{e}^{(1+c_j)\tau\kappa}\big[\mathcal{L}u_{n,j}+\mathcal{N}(u_{n,j})+\kappa u_{n,j}\big]\right),\\&i=1,\ldots,s.\end{aligned}\tag{3.7}$$

It can be directly derived that the modification (3.7) conserves mass (Principle 1) for the RSLM formulation.

By substituting stage solutions into $\kappa u_{n,j}$, we obtain

$$u_{n,i}=\sum_{j=-1}^{0}\hat{d}_{i,j}(\tau\kappa)u_{n,j}+\tau\sum_{j=-1}^{i-1}\hat{a}_{i,j}(\tau\kappa)\big[\mathcal{L}u_{n,j}+\mathcal{N}(u_{n,j})\big],\quad i=1,\ldots,s,\tag{3.8}$$

where $\hat{d}_{i,j}(\tau\kappa)$ and $\hat{a}_{i,j}(\tau\kappa)$ are recurrently computed by

$$\begin{aligned}&\hat{d}_{i,j}(\tau\kappa)=\frac{1}{\psi_i(\tau\kappa)}\left[d_{ij}\mathrm{e}^{(1+c_j)\tau\kappa}+\tau\kappa\sum_{k=-1}^{i-1}a_{i,k}\mathrm{e}^{(1+c_k)\tau\kappa}\hat{d}_{k,j}(\tau\kappa)\right],\\&i=-1,\ldots,s,\quad j=-1,0,\\&\hat{a}_{i,j}(\tau\kappa)=\frac{1}{\psi_i(\tau\kappa)}\left[a_{i,j}\mathrm{e}^{(1+c_j)\tau\kappa}+\tau\kappa\sum_{k=1}^{i-1}a_{i,k}\mathrm{e}^{(1+c_k)\tau\kappa}\hat{a}_{k,j}(\tau\kappa)\right],\\&i=1,\ldots,s,\quad j=-1,\ldots,i-1.\end{aligned}\tag{3.9}$$

We denote the formulation (3.8) with new coefficients $\hat{d}_{i,j},\hat{a}_{i,j}$ and old abscissas c_i as the first parametric TSRK method (pTSRK1).

3.2 Second parametric two-step Runge-Kutta method

The exponential term $e^{(1+c_j)\tau\kappa}$ will be extremely large and may blow up when $\tau\kappa\gg 0$. To improve the numerical stability, we propose a new recurrent approximation to conserve the mass. Denote

$$\phi_k(z):=1+z+\cdots+\frac{1}{k!}z^k$$

as the k-th order Taylor polynomial approximation to the exponential function e^z. Letting

$$\psi_j(\tau\kappa):=\phi_{p-1}\big((1+c_j)\tau\kappa\big),\quad j=-1,0,$$

we approximate $e^{(1+c_i)\tau\kappa}$ recurrently using

$$\psi_i(\tau\kappa):=\sum_{j=-1}^{0}d_{i,j}\psi_j(\tau\kappa)+\tau\kappa\sum_{j=-1}^{i-1}a_{i,j}\psi_j(\tau\kappa),\quad i=1,\dots,s. \tag{3.10}$$

Then, the second improvement of (3.4) is obtained as

$$u_{n,i}=\frac{1}{\psi_i(\tau\kappa)}\left(\sum_{j=-1}^{0}d_{i,j}\psi_j(\tau\kappa)u_{n,j}+\tau\sum_{j=-1}^{i-1}a_{i,j}\psi_j(\tau\kappa)\big[\mathcal{L}u_{n,j}+\mathcal{N}(u_{n,j})+\kappa u_{n,j}\big]\right) \tag{3.11}$$

$$=\sum_{j=-1}^{0}\hat{d}_{i,j}(\tau\kappa)u_{n,j}+\tau\sum_{j=-1}^{i-1}\hat{a}_{i,j}(\tau\kappa)\big[\mathcal{L}u_{n,j}+\mathcal{N}(u_{n,j})\big],\quad i=1,\dots,s, \tag{3.12}$$

where

$$\begin{aligned}
&\hat{d}_{i,j}(\tau\kappa)=\frac{1}{\psi_i(\tau\kappa)}\left[d_{ij}\psi_j(\tau\kappa)+\tau\kappa\sum_{k=-1}^{i-1}a_{i,k}\psi_k(\tau\kappa)\hat{d}_{k,j}(\tau\kappa)\right],\\
&i=-1,\dots,s,\quad j=-1,0,\\
&\hat{a}_{i,j}(\tau\kappa)=\frac{1}{\psi_i(\tau\kappa)}\left[a_{i,j}\psi_j(\tau\kappa)+\tau\kappa\sum_{k=1}^{i-1}a_{i,k}\psi_k(\tau\kappa)\hat{a}_{k,j}(\tau\kappa)\right],\\
&i=1,\dots,s,\quad j=-1,\dots,i-1.
\end{aligned} \tag{3.13}$$

We denote the formulation (3.12) with new coefficients $\hat{d}_{i,j}$ and $\hat{a}_{i,j}$ given by (3.13) and the old abscissas c_i as pTSRK2.

Remark 3.1. To design conservative approximations for the IFTSRK method (3.4), different decompositions of exponential functions may be used. The decomposition of $e^{-(c_i-c_j)\tau\kappa}$ into $e^{-(1+c_i)\tau\kappa}e^{(1+c_j)\tau\kappa}$ has the advantage that we can present the two modifications in a unified framework. Indeed, for the pTSRK1 method, the modifications using the decompositions $e^{-(1+c_i)\tau\kappa}e^{(1+c_j)\tau\kappa}$ and $e^{-c_i\tau\kappa}e^{c_j\tau\kappa}$ are equivalent. However, the decomposition $e^{-c_i\tau\kappa}e^{c_j\tau\kappa}$ can not be used in the pTSRK2 method. The reason is that, to preserve the maximum principle, we have to make sure that the approximations $\psi_j(\tau\kappa), j=$

$-1,\ldots,s$ are positive. Noting that the abscissa $c_{-1}=-1$, when approximating $e^{c_{-1}\tau\kappa}$ using a k-th order Taylor expansion, the positiveness of function $\psi_{-1}(\tau\kappa):=\phi_k(c_{-1}\tau\kappa)$ can not be guaranteed. In practice, for the pTSRK2 method, the approximations to $e^{(1+c_j)\tau\kappa}$, $j=-1,0$ can be replaced by any k-th order ($k\geq p-1$) Taylor expansions; the higher is the order, the better is the accuracy of the approximations.

3.3 Accuracy of parametric two-step Runge-Kutta schemes

To derive order conditions for modifications (3.7) and (3.11), we define

$$\hat{c}_i=-\hat{d}_{i,-1}+\sum_{j=-1}^{i-1}\hat{a}_{i,j},\quad i=-1,\ldots,s,$$

and present the pTSRK1/2 schemes using a unified Butcher-like tableau

$$\begin{array}{cc|c|c} c & \hat{c} & \hat{D} & \hat{A} \\ \hline c_s & \hat{c}_s & \hat{\theta}^T & \hat{b}^T \end{array}=\begin{array}{cc|cc|cccccc} c_{-1} & \hat{c}_{-1} & 1 & 0 & 0 & & & & \\ c_0 & \hat{c}_0 & 0 & 1 & 0 & 0 & & & \\ c_1 & \hat{c}_1 & \hat{d}_{1,-1} & \hat{d}_{1,0} & \hat{a}_{1,-1} & \hat{a}_{1,0} & 0 & & \\ \vdots & \vdots & \vdots & \vdots & \vdots & \vdots & \ddots & \ddots & \\ c_{s-1} & \hat{c}_{s-1} & \hat{d}_{s-1,-1} & \hat{d}_{s-1,0} & \hat{a}_{s-1,-1} & \hat{a}_{s-1,0} & \hat{a}_{s-1,1} & \cdots & 0 \\ \hline c_s & \hat{c}_s & \hat{d}_{s,-1} & \hat{d}_{s,0} & \hat{a}_{s,-1} & \hat{a}_{s,0} & \hat{a}_{s,1} & \cdots & \hat{a}_{s,s-1} \end{array}. \tag{3.14}$$

Let $\ell=[1,0]^T$ and denote $g(t,u):=\mathcal{L}u+\mathcal{N}(u)$. We apply the Taylor expansions to obtain

$$u(t_{n,i})=u(t_n)+\sum_{k=1}^{p}\frac{(c_i\tau)^k}{k!}\left[\frac{\partial}{\partial t}+g\frac{\partial}{\partial u}\right]^{(k-1)}g|_{t_n,u(t_n)}+\mathcal{O}(\tau^{p+1}),\quad i=-1,\ldots,s, \tag{3.15}$$

$$\begin{aligned} &g\left(t_{n,j},\sum_{l=-1}^{0}\hat{d}_{j,l}u(t_{n,l})+\tau\sum_{l=-1}^{j-1}\hat{a}_{j,l}g\big(t_{n,l},u(t_{n,l})\big)\right)\\ &=\sum_{k=1}^{p}\frac{\tau^{k-1}}{(k-1)!}\left[c_j\frac{\partial}{\partial t}+\left[-\hat{d}_{j,-1}\hat{g}\big(t_{n,-1},u(t_{n,-1})\big)+\sum_{l=-1}^{j-1}\hat{a}_{j,l}\hat{g}\big(t_{n,l},u(t_{n,l})\big)\right]\frac{\partial}{\partial u}\right]^{(k-1)}g\big|_{t_n,u(t_n)}\\ &\quad+\mathcal{O}(\tau^p),\quad j=-1,\ldots,s, \end{aligned} \tag{3.16}$$

where $\hat{g}(t_{n,l},u(t_{n,l}))$ denotes the Taylor expansion of $g(t_{n,l},u(t_{n,l}))$ at (t_n,u_n).

Inserting the exact solutions into the numerical scheme (3.8) (or (3.12)) gives

$$\begin{aligned} u(t_{n,i})=&\sum_{j=-1}^{0}\hat{d}_{i,j}u(t_{n,j})+\tau\sum_{j=-1}^{i-1}\hat{a}_{i,j}g\left(t_{n,j},\sum_{l=-1}^{0}\hat{d}_{j,l}u(t_{n,l})+\tau\sum_{l=-1}^{j-1}\hat{a}_{j,l}g\big(t_{n,l},u(t_{n,l})\big)\right)\\ &+\Delta_{n,i},\quad i=-1,\ldots,s. \end{aligned} \tag{3.17}$$

Substituting (3.15)-(3.16) into (3.17) gives the defects

$$\begin{aligned}\Delta_{n,i}=\sum_{k=1}^{p}\tau^k\Bigg(&\frac{1}{k!}\big(c_i^k-\hat{d}_{i,-1}(-1)^k\big)\left[\frac{\partial}{\partial t}+g\frac{\partial}{\partial u}\right]^{(k-1)}\\&-\frac{1}{(k-1)!}\sum_{j=-1}^{i-1}\hat{a}_{i,j}\Bigg[c_j\frac{\partial}{\partial t}+\Bigg[-\hat{d}_{j,-1}\hat{g}\big(t_{n,-1},u(t_{n,-1})\big)\\&+\sum_{l=-1}^{j-1}\hat{a}_{j,l}\hat{g}\big(t_{n,l},u(t_{n,l})\big)\Bigg]\frac{\partial}{\partial u}\Bigg]^{(k-1)}\Bigg)g|_{t_n,u(t_n)}\\&+\mathcal{O}(\tau^{p+1}),\quad i=-1,\dots,s.\end{aligned}$$

Then, it can be concluded that the order conditions will contain both c_i and $\hat{c}_i$. We define

$$\begin{aligned}&\tilde{c}_{j,m}^k=c_j^m\hat{c}_j^{k-m},\quad \tilde{c}_m^k=\big[\tilde{c}_{-1,m}^k,\tilde{c}_{0,m}^k,\cdots,\tilde{c}_{s-1,m}^k\big]^T,\quad \tilde{C}_m^k=\mathrm{diag}(\tilde{c}_m^k),\quad m=0,\dots,k,\\&\hat{\tau}_{i,k,m}=\frac{1}{k!}\big(c_i^k-\hat{d}_{i,-1}(-1)^k\big)-\frac{1}{(k-1)!}\sum_{j=-1}^{i-1}\hat{a}_{i,j}\tilde{c}_{j,m}^{k-1},\qquad m=0,\dots,k-1,\end{aligned}$$

and denote $\hat{\tau}_{k,m}=[\hat{\tau}_{-1,k,m},\hat{\tau}_{0,k,m},\cdots,\hat{\tau}_{s-1,k,m}]^T$. By using the parametric Butcher tableau (3.14), we obtain

$$\begin{aligned}\hat{\tau}_{k,m}&=\frac{1}{k!}\big(c^k-\hat{D}(-\ell)^k\big)-\frac{1}{(k-1)!}\hat{A}\tilde{c}_m^{k-1},\\\hat{\tau}_{s,k,m}&=\frac{1}{k!}\big(1-\hat{\theta}^T(-\ell)^k\big)-\frac{1}{(k-1)!}\hat{b}^T\tilde{c}_m^{k-1}.\end{aligned}\tag{3.18}$$

The research of the TSRK [47] shows that the explicit TSRK with non-negative Butcher coefficients has an eighth-order barrier. Thus, pTSRK1/2 with non-negative Butcher coefficients can reach, at most, eighth-order. Following [47] and letting $z:=\tau\kappa$ and $\mathbf{1}_s=[1,1,\cdots,1]^T\in\mathbb{R}^s$, we present the order conditions for the parametric Butcher tableau from first- to eighth-order using (3.18), as follows:

Order 1: $\hat{b}^T\mathbf{1}_{s+1}-(1+\hat{\theta}^T\ell)=\mathcal{O}(z^p)$.

Order 2: $\hat{b}^T\tilde{c}_m-\dfrac{1-\hat{\theta}^T\ell^2}{2}=\mathcal{O}(z^{p-1})$.

Order 3: $\hat{b}^T\tilde{c}_m^2-\dfrac{1+\hat{\theta}^T\ell^3}{3}=\mathcal{O}(z^{p-2})$, $\quad\hat{b}^T\hat{\boldsymbol{\tau}}_{2,m}=\mathcal{O}(z^{p-2})$.

Order 4: $\hat{b}^T\tilde{c}_m^3-\dfrac{1-\hat{\theta}^T\ell^4}{4}=\mathcal{O}(z^{p-3})$, $\quad\hat{b}^T\hat{A}\hat{\boldsymbol{\tau}}_{2,m}=\mathcal{O}(z^{p-3})$,

$\hat{b}^T\tilde{C}_{m_1}\hat{\boldsymbol{\tau}}_{2,m_2}=\mathcal{O}(z^{p-3})$, $\quad\hat{b}^T\hat{\boldsymbol{\tau}}_{3,m}=\mathcal{O}(z^{p-3})$.

Order 5: $\hat{b}^T\tilde{c}_m^4-\dfrac{1+\hat{\theta}^T\ell^5}{5}=\mathcal{O}(z^{p-4})$, $\quad\hat{b}^T\hat{A}\hat{\boldsymbol{\tau}}_{3,m}=\mathcal{O}(z^{p-4})$,

$$\hat{b}^T\tilde{C}_{m_1}\hat{\boldsymbol{\tau}}_{3,m_2}=\mathcal{O}(z^{p-4}),\qquad \hat{b}^T\hat{\boldsymbol{\tau}}_{4,m}=\mathcal{O}(z^{p-4}),$$
$$\hat{\boldsymbol{\tau}}_{2,m}=\mathcal{O}(z^{\lceil\frac{p-4}{2}\rceil}).$$

Order 6:
$$\hat{b}^T\tilde{c}_m^5-\frac{1-\hat{\theta}^T\ell^6}{6}=\mathcal{O}(z^{p-5}),\qquad \hat{b}^T\hat{A}\hat{\boldsymbol{\tau}}_{4,m}=\mathcal{O}(z^{p-5}),$$
$$\hat{b}^T\tilde{C}_{m_1}\hat{\boldsymbol{\tau}}_{4,m_2}=\mathcal{O}(z^{p-5}),\qquad \hat{b}^T\hat{\boldsymbol{\tau}}_{5,m}=\mathcal{O}(z^{p-5}),$$
$$\hat{b}^T\hat{A}^2\hat{\boldsymbol{\tau}}_{3,m}=\mathcal{O}(z^{p-5}),\qquad \hat{b}^T\hat{A}\tilde{C}_{m_1}\hat{\boldsymbol{\tau}}_{3,m_2}=\mathcal{O}(z^{p-5}),$$
$$\hat{b}^T\tilde{C}_{m_1}\hat{A}\hat{\boldsymbol{\tau}}_{3,m_2}=\mathcal{O}(z^{p-5}),\qquad \hat{b}^T\tilde{C}_{m_1}^2\hat{\boldsymbol{\tau}}_{3,m_2}=\mathcal{O}(z^{p-5}).$$

Order 7:
$$\hat{b}^T\tilde{c}_m^6-\frac{1+\hat{\theta}^T\ell^7}{7}=\mathcal{O}(z^{p-6}),\qquad \hat{b}^T\hat{A}\hat{\boldsymbol{\tau}}_{5,m}=\mathcal{O}(z^{p-6}),$$
$$\hat{b}^T\tilde{C}_{m_1}\hat{\boldsymbol{\tau}}_{5,m_2}=\mathcal{O}(z^{p-6}),\qquad \hat{b}^T\hat{\boldsymbol{\tau}}_{6,m}=\mathcal{O}(z^{p-6}),$$
$$\hat{b}^T\hat{A}^2\hat{\boldsymbol{\tau}}_{4,m}=\mathcal{O}(z^{p-6}),\qquad \hat{b}^T\hat{A}\tilde{C}_{m_1}\hat{\boldsymbol{\tau}}_{4,m_2}=\mathcal{O}(z^{p-6}),$$
$$\hat{b}^T\tilde{C}_{m_1}\hat{A}\hat{\boldsymbol{\tau}}_{4,m_2}=\mathcal{O}(z^{p-6}),\qquad \hat{b}^T\tilde{C}_{m_1}^2\hat{\boldsymbol{\tau}}_{4,m_2}=\mathcal{O}(z^{p-6}),$$
$$\hat{\boldsymbol{\tau}}_{3,m}=\mathcal{O}(z^{\lceil\frac{p-6}{2}\rceil}).$$

Order 8:
$$\hat{b}^T\tilde{c}_m^7-\frac{1-\hat{\theta}^T\ell^8}{8}=\mathcal{O}(z^{p-7}),\qquad \hat{b}^T\hat{A}\hat{\boldsymbol{\tau}}_{6,m}=\mathcal{O}(z^{p-7}),$$
$$\hat{b}^T\tilde{C}_{m_1}\hat{\boldsymbol{\tau}}_{6,m_2}=\mathcal{O}(z^{p-7}),\qquad \hat{b}^T\hat{\boldsymbol{\tau}}_{7,m}=\mathcal{O}(z^{p-7}),$$
$$\hat{b}^T\hat{A}^3\hat{\boldsymbol{\tau}}_{4,m}=\mathcal{O}(z^{p-7}),\qquad \hat{b}^T\hat{A}^2\hat{\boldsymbol{\tau}}_{5,m}=\mathcal{O}(z^{p-7}),$$
$$\hat{b}^T\hat{A}^2\tilde{C}_{m_1}\hat{\boldsymbol{\tau}}_{4,m_2}=\mathcal{O}(z^{p-7}),\qquad \hat{b}^T\hat{A}\tilde{C}_{m_1}\hat{A}\hat{\boldsymbol{\tau}}_{4,m_2}=\mathcal{O}(z^{p-7}),$$
$$\hat{b}^T\hat{A}\tilde{C}_{m_1}\hat{\boldsymbol{\tau}}_{5,m_2}=\mathcal{O}(z^{p-7}),\qquad \hat{b}^T\hat{A}\tilde{C}_{m_1}^2\hat{\boldsymbol{\tau}}_{4,m_2}=\mathcal{O}(z^{p-7}),$$
$$\hat{b}^T\tilde{C}_{m_1}\hat{A}^2\hat{\boldsymbol{\tau}}_{4,m_2}=\mathcal{O}(z^{p-7}),\qquad \hat{b}^T\tilde{C}_{m_1}\hat{A}\hat{\boldsymbol{\tau}}_{5,m_2}=\mathcal{O}(z^{p-7}),$$
$$\hat{b}^T\tilde{C}_{m_1}\hat{A}\hat{C}_{m_2}\hat{\boldsymbol{\tau}}_{4,m_3}=\mathcal{O}(z^{p-7}),\qquad \hat{b}^T\tilde{C}_{m_1}^2\hat{A}\hat{\boldsymbol{\tau}}_{4,m_2}=\mathcal{O}(z^{p-7}),$$
$$\hat{b}^T\tilde{C}_{m_1}^2\hat{\boldsymbol{\tau}}_{5,m_2}=\mathcal{O}(z^{p-7}),\qquad \hat{b}^T\tilde{C}_{m_1}^3\hat{\boldsymbol{\tau}}_{4,m_2}=\mathcal{O}(z^{p-7}).$$

To have p-th order accuracy, the pTSRK method should satisfy all previous order conditions as well as additional conditions for each order. We consider the pTSRK2(2,2) scheme to illustrate that the proposed modification retains the order of the underlying TSRK scheme.

The parametric coefficients of pTSRK(2,2) are computed as follows:

$$\begin{aligned}
&\psi_{-1}=1,\quad \psi_0=\phi_1\big((1+c_0)z\big)=1+z,\\
&\psi_1=d_{1,-1}\psi_{-1}+d_{1,0}\psi_0+z[a_{1,-1}\psi_{-1}+a_{1,0}\psi_0]=1+z(1+c_1)+z^2a_{1,0},\\
&\psi_2=d_{2,-1}\psi_{-1}+d_{2,0}\psi_0+z[a_{2,-1}\psi_{-1}+a_{2,0}\psi_0+a_{2,1}\psi_1]\\
&\quad=1+z(1+c_2)+z^2\big[a_{2,0}+a_{2,1}(1+c_1)\big]+z^3a_{2,1}a_{1,0},\\
&\hat{d}_{-1,-1}=d_{-1,-1},\quad \hat{d}_{0,-1}=0,\quad \hat{d}_{1,-1}=\frac{1}{\psi_1}(d_{1,-1}+za_{1,-1}),
\end{aligned}$$

$$\hat{a}_{1,-1}=\frac{1}{\psi_1}a_{1,-1},\quad \hat{a}_{1,0}=\frac{1}{\psi_1}a_{1,0}\psi_0,$$
$$\hat{c}_1=\frac{1}{\psi_1}\left[a_{1,-1}+a_{1,0}(1+z)-d_{1,-1}-za_{1,-1}\right]=\frac{c_1+z(a_{1,0}-a_{1,-1})}{1+z(1+c_1)+z^2a_{1,0}},$$
$$\begin{aligned}\hat{d}_{2,-1}&=\frac{1}{\psi_2}\left[d_{2,-1}\psi_{-1}+z(a_{2,-1}\psi_{-1}\hat{d}_{-1,-1}+a_{2,0}\psi_0\hat{d}_{0,-1}+a_{2,1}\psi_1\hat{d}_{1,-1})\right]\\&=\frac{1}{\psi_2}\left[d_{2,-1}+z(a_{2,-1}+a_{2,1}d_{1,-1})+z^2a_{2,1}a_{1,-1}\right],\end{aligned}$$
$$\hat{a}_{2,-1}=\frac{1}{\psi_2}[a_{2,-1}\psi_{-1}+za_{2,1}\psi_1\hat{a}_{1,-1}]=\frac{1}{\psi_2}[a_{2,-1}+za_{2,1}a_{1,-1}],$$
$$\hat{a}_{2,0}=\frac{1}{\psi_2}\left[a_{2,0}\psi_0+z(a_{2,1}a_{1,0}\psi_0)\right]=\frac{1}{\psi_2}\left[a_{2,0}+z(a_{2,0}+a_{2,1}a_{1,0})+z^2a_{2,1}a_{1,0}\right],$$
$$\hat{a}_{2,1}=\frac{1}{\psi_2}[a_{2,1}\psi_1]=\frac{1}{\psi_2}\left[a_{2,1}+za_{2,1}(1+c_1)+z^2a_{2,1}a_{1,0}\right].$$

Ketcheson *et al.* [47] and Isherwood *et al.* [40] showed that TSRK(2,2) satisfies the order conditions

$$c_2=b^T\mathbf{1}_s-\theta^T\ell=\sum_{j=-1}^{1}a_{2,j}-d_{2,-1}=1,$$
$$b^Tc-\frac{c_2-\theta^T\ell^2}{2}=-a_{2,-1}+a_{2,1}c_1-\frac{1-d_{2,-1}}{2}=0.$$

Then, the verification of the pTSRK(2,2) scheme is performed as follows:

$$\begin{aligned}\hat{c}_2&=\frac{1+z\left(a_{2,1}a_{1,-1}+a_{2,0}+a_{2,1}a_{1,0}+a_{2,1}(1+c_1)-a_{2,-1}-a_{2,1}d_{1,-1}\right)+z^2(2a_{2,1}a_{1,0}-a_{2,1}a_{1,-1})}{1+(1+c_2)z+z^2\left[a_{2,0}+a_{2,1}(1+c_1)\right]+z^3a_{2,1}a_{1,0}}\\&=\frac{1+z(1+c_2)+z^2(2a_{2,1}a_{1,0}-a_{2,1}a_{1,-1})}{1+(1+c_2)z+z^2\left[a_{2,0}+a_{2,1}(1+c_1)\right]+z^3a_{2,1}a_{1,0}}=1+\mathcal{O}(z^2),\end{aligned}$$
$$\hat{b}^T\hat{c}-\frac{1-\hat{d}_{2,-1}}{2}=\hat{a}_{2,-1}\hat{c}_{-1}+\hat{a}_{2,0}\hat{c}_0+\hat{a}_{2,1}\hat{c}_1-\frac{1-\left(d_{2,-1}+\mathcal{O}(z)\right)}{2}=\mathcal{O}(z),$$
$$\hat{b}^Tc-\frac{1-\hat{d}_{2,-1}}{2}=\hat{a}_{2,-1}c_{-1}+\hat{a}_{2,0}c_0+\hat{a}_{2,1}c_1-\frac{1-\left(d_{2,-1}+\mathcal{O}(z)\right)}{2}=\mathcal{O}(z).$$

The order verification processes of other pTSRK1/2 schemes are more complex. By performing tedious Taylor expansions using the MATLAB code in a public repository [74], we verified that the pTSRK1/2 schemes with underlying TSRK coefficients presented in [27, 40] satisfy the order conditions listed above. Then, we have the following corollary.

Corollary 3.1. *Assume* $u(t,x)\in C^{p+1}([0,T];C^2(\bar{\Omega}))$ *is the exact solution to* (2.1), *and* $u^{n+j}=u(t^{n+j}), j=-1,0$. *Then, the solution* u^{n+1} *obtained by* pTSRK1 (3.8) *or* pTSRK2 (3.12) *with an*

underlying TSRK*(s,p) Butcher tableau provided by* [40] *has a* $(p+1)$*-th order truncation error, i.e.,*

$$u(t^n+\tau)-u^{n+1}=\mathcal{O}\left(\tau^{p+1}\sum_{k=0}^{p}\kappa^k\right)=\mathcal{O}(\tau^{p+1}).$$

Proof. In the above error expansion, we can see that each of the residuals in $\Delta_{n,s}$ is multiplied by the corresponding $\mathcal{O}(\tau^k)$ term. Performing a summation gives the overall truncation error $\mathcal{O}(\tau^{p+1}\sum_{k=0}^{p}\kappa^k)$, which is still $\mathcal{O}(\tau^{p+1})$. □

3.4 Properties of pTSRK schemes

In addition to the conservation of mass for the RSLM formulation, as an improvement over the traditional IFTSRK method (3.4), we show that the pTSRK1/2 schemes preserve the fixed points of the system.

Lemma 3.1. *The* pTSRK1 (3.8) *with coefficients* $\hat{d}_{i,j},\hat{a}_{i,j}$ (3.9)*, and the* pTSRK2 (3.12) *with coefficients* $\hat{d}_{i,j},\hat{a}_{i,j}$ (3.13)*, preserve the fixed points of* (2.1) *in the sense that if there exists a* u^* *such that*

$$Lu^*+\mathcal{N}(u^*)=0, \tag{3.19}$$

then the solution of pTSRK1/2 *satisfies* $u^{n+1}=u^*$*, on the condition that* $u^n=u^{n-1}=u^*$*.*

Proof. Consider the pTSRK1 as an example. We first show that $\sum_{j=-1}^{0}\hat{d}_{i,j}=1, i=-1,0,\ldots,s$ using mathematical induction.

Note that $\sum_{j=-1}^{0}\hat{d}_{k,j}=1, k=-1,0$. Assuming that $\sum_{j=-1}^{0}\hat{d}_{k,j}=1, k=1,\ldots,i-1$, we only need to prove that $\sum_{j=-1}^{0}\hat{d}_{i,j}=1, i\le s$. By using definitions of $\psi_i(\tau\kappa)$ and conditions $\sum_{j=-1}^{0}d_{i,j}=1, i=1,\ldots,s$, we obtain

$$\begin{aligned}\sum_{j=-1}^{0}\hat{d}_{i,j}&=\frac{1}{\psi_i(\tau\kappa)}\left[\sum_{j=-1}^{0}d_{i,j}\mathrm{e}^{(1+c_j)\tau\kappa}+\tau\kappa\sum_{k=-1}^{i-1}a_{i,k}\mathrm{e}^{(1+c_k)\tau\kappa}\sum_{j=-1}^{0}\hat{d}_{k,j}\right]\\&=\frac{1}{\psi_i(\tau\kappa)}\left[\sum_{j=-1}^{0}d_{i,j}\mathrm{e}^{(1+c_j)\tau\kappa}+\tau\kappa\sum_{k=-1}^{i-1}a_{i,k}\mathrm{e}^{(1+c_k)\tau\kappa}\right]=1,\quad i\le s.\end{aligned}$$

Assuming that $u_{n,j}=u^*, j=1,\ldots,i-1$, we have

$$u_{n,i}=\sum_{j=-1}^{0}\hat{d}_{i,j}u_{n,j}+\tau\sum_{j=-1}^{i-1}\hat{a}_{i,j}\underbrace{\left(Lu_{n,j}+\mathcal{N}(u_{n,j})\right)}_{=0}=\sum_{j=-1}^{0}\hat{d}_{i,j}u^*=u^*,\quad i\le s.$$

Then we obtain $u^{n+1}=u_{n,s}=u^*$. The proof for the pTSRK2 can be carried out similarly. □

3.5 Parametric integrating factor TSRK schemes for stiff systems

The explicit treatment of the stiff terms in pTSRK1/2 schemes leads to severe time-step restriction. To overcome this shortcoming, we show that under certain requirements of the TSRK Butcher tableau and the stabilization parameter κ, by treating the nonlinear term explicitly (Principle 2), the pTSRK1/2 schemes together with an integrating factor $\mathrm{e}^{-t\mathcal{L}}$ can preserve the maximum principle for any time-step size (Principle 3).

Assumption 3.1. The underlying TSRK Butcher tableau satisfies the following:

1) non-negative coefficients:

$$\begin{aligned} &d_{i,j}\geq 0, \quad i=-1,0,\ldots,s, \quad j=-1,0,\\ &a_{i,j}\geq 0, \quad i=-1,0,\ldots,s, \quad j=-1,\ldots,i-1; \end{aligned}$$

2) non-decreasing abscissas: $-1=c_{-1}\leq c_0\leq\cdots\leq c_s=1$.

By applying the integrating factor method (integrating factor being $\mathrm{e}^{-t\mathcal{L}}$) with the underlying pTSRK1/2 schemes to (2.1), we obtain pIFTSRK1 ($\hat{d}_{i,j},\hat{a}_{i,j}$ given by (3.9), $\psi_i(\tau\kappa)$ given by (3.6))

$$u_{n,i}=\sum_{j=-1}^{0}\hat{d}_{i,j}\mathrm{e}^{(c_i-c_j)\tau\mathcal{L}}u_{n,j}+\tau\sum_{j=-1}^{i-1}\hat{a}_{i,j}\mathrm{e}^{(c_i-c_j)\tau\mathcal{L}}\mathcal{N}(u_{n,j}) \tag{3.20}$$

$$=\frac{1}{\psi_i(\tau\kappa)}\left[\sum_{j=-1}^{0}d_{i,j}\mathrm{e}^{(1+c_j)\tau\kappa}\mathrm{e}^{(c_i-c_j)\tau\mathcal{L}}u_{n,j}+\tau\sum_{j=-1}^{i-1}a_{i,j}\mathrm{e}^{(1+c_j)\tau\kappa}\mathrm{e}^{(c_i-c_j)\tau\mathcal{L}}\mathcal{N}_\kappa(u_{n,j})\right], \tag{3.21}$$

$i=1,\ldots,s,$

and pIFTSRK2 ($\hat{d}_{i,j},\hat{a}_{i,j}$ given by (3.13), $\psi_i(\tau\kappa)$ given by (3.10))

$$u_{n,i}=\frac{1}{\psi_i(\tau\kappa)}\left[\sum_{j=-1}^{0}d_{i,j}\psi_j(\tau\kappa)\mathrm{e}^{(c_i-c_j)\tau\mathcal{L}}u_{n,j}+\tau\sum_{j=-1}^{i-1}a_{i,j}\psi_j(\tau\kappa)\mathrm{e}^{(c_i-c_j)\tau\mathcal{L}}\mathcal{N}_\kappa(u_{n,j})\right], \tag{3.22}$$

$i=1,\ldots,s.$

Theorem 3.1. *Assume κ satisfies condition* (2.6) *and the underlying* TSRK *Butcher tableau of* pIFTSRK1/2 *satisfies Assumption* 3.1. *Then, for the system* (2.1), *if the starting values satisfy $\|u^j\|_{L^\infty}\leq\beta, j=0,1$, the solutions obtained from* pIFTSRK1/2 *satisfy $\|u^{n+1}\|_{L^\infty}\leq\beta$ for any $\tau>0$, $n\geq 1$.*

Proof. We prove this claim by induction. Consider the equivalent formulation (3.21) of pIFTSRK1 as an example. Assuming that $\|u_{n,j}\|_{L^\infty}\leq\beta, j=-1,\ldots,i-1$, we verify that the maximum principle holds for $u_{n,i}$.

Using Lemmas 2.1 and 2.4, the conditions in Assumption 3.1, and the definitions of $\psi_i(\tau\kappa)$, we have

$$\begin{aligned}\|u_{n,i}\|_{L^\infty} &\le \frac{1}{\psi_i(\tau\kappa)}\left[\sum_{j=-1}^{0} d_{i,j}\mathrm{e}^{(1+c_j)\tau\kappa}\|\mathrm{e}^{(c_i-c_j)\tau\mathcal{L}}u_{n,j}\|_{L^\infty}\right.\\ &\qquad\left.+\tau\sum_{j=-1}^{i-1} a_{i,j}\mathrm{e}^{(1+c_j)\tau\kappa}\|\mathrm{e}^{(c_i-c_j)\tau\mathcal{L}}\mathcal{N}_\kappa(u_{n,j})\|_{L^\infty}\right]\\ &\le \frac{1}{\psi_i(\tau\kappa)}\left[\sum_{j=-1}^{0} d_{i,j}\mathrm{e}^{(1+c_j)\tau\kappa}+\tau\kappa\sum_{j=-1}^{i-1} a_{i,j}\mathrm{e}^{(1+c_j)\tau\kappa}\right]\beta=\beta,\quad i\le s.\end{aligned}$$

Then, we have $\|u^{n+1}\|_{L^\infty}=\|u_{n,s}\|_{L^\infty}\le\beta$. □

Finally, we show that pIFTSRK1/2 conserve the mass (Principle 1) of the RSLM formulation under periodic or homogeneous Neumann boundary conditions.

Theorem 3.2. *Assume that the underlying* TSRK *Butcher tableau satisfies Assumption* 3.1. *If starting values satisfy* $M(u^1)=M(u^0)=M^0$, *then* pIFTSRK1/2 *conserve the mass of the* RSLM *formulation under periodic or homogeneous Neumann boundary conditions.*

Proof. We prove this claim by mathematical induction. Assume $(u_{n,j},1)=M^0$, $j=-1,\ldots,i-1$. By taking the L^2 inner product on both sides of (3.20) with 1, and using Lemma 2.2 and the equality

$$(\mathcal{N}(u_{n,j}),1)=\int_\Omega\left[f(u_{n,j})-\frac{1}{|\Omega|}\int_\Omega f(u_{n,j})\mathrm{d}x\right]\mathrm{d}x=0,$$

we have

$$\begin{aligned}(u_{n,i},1)&=\sum_{j=-1}^{0}\hat{d}_{i,j}\big(\mathrm{e}^{(c_i-c_j)\tau\mathcal{L}}u_{n,j},1\big)+\tau\sum_{j=-1}^{i-1}\hat{a}_{i,j}\big(\mathrm{e}^{(c_i-c_j)\tau\mathcal{L}}\mathcal{N}(u_{n,j}),1\big)\\ &=\sum_{j=-1}^{0}\hat{d}_{i,j}(u_{n,j},1)+\tau\sum_{j=-1}^{i-1}\hat{a}_{i,j}\big(\mathcal{N}(u_{n,j}),1\big)=M^0,\quad i\le s.\end{aligned}$$

Then, we have $M^{n+1}=(u_{n,s},1)=M^0$. □

Remark 3.2. The pIFTSRK1/2 can be seen as improvements over the stabilized IFTSRK method (with integrating factor $\mathrm{e}^{-t\mathcal{L}_\kappa}$, denoted as sIFTSRK)

$$\text{sIFTSRK:}\quad u_{n,i}=\sum_{j=-1}^{0} d_{i,j}\mathrm{e}^{(c_i-c_j)\tau\mathcal{L}_\kappa}u_{n,j}+\tau\sum_{j=-1}^{i-1} a_{i,j}\mathrm{e}^{(c_i-c_j)\tau\mathcal{L}_\kappa}\mathcal{N}_\kappa(u_{n,j}),\quad i=1,\ldots,s. \tag{3.23}$$

Under condition (2.6) and Assumption 3.1, assuming that $\|u_{n,j}\|_{L^\infty} \le \beta$, $j=-1,\ldots,i-1$, taking the L^∞-norm on both sides of (3.23) and applying Lemma 2.1 yields

$$\|u_{n,i}\|_{L^\infty} \le \mathrm{e}^{-(1+c_i)\tau\kappa}\left[\sum_{j=-1}^{0} d_{i,j}\mathrm{e}^{(1+c_j)\tau\kappa} + \tau\kappa\sum_{j=-1}^{i-1} a_{i,j}\mathrm{e}^{(1+c_j)\tau\kappa}\right]\beta, \quad i\le s.$$

We define the amplification function of the i-th stage of the sIFTSRK (3.23) as

$$g_i(\tau\kappa) := \mathrm{e}^{-(1+c_i)\tau\kappa}\left[\sum_{j=-1}^{0} d_{i,j}\mathrm{e}^{(1+c_j)\tau\kappa} + \tau\kappa\sum_{j=-1}^{i-1} a_{i,j}\mathrm{e}^{(1+c_j)\tau\kappa}\right], \quad i=1,\ldots,s.$$

To preserve the maximum principle unconditionally, the inequalities $g_i(\tau\kappa)\le 1, i=1,\ldots,s$ should hold for any $\tau\kappa > 0$. However, by checking all underlying non-negative TSRK Butcher tableaux developed by Isherwood *et al.* [27,40], we find that [74] only the second-order sIFTSRK(s,2) ($s=2,\ldots,10$) and the third-order sIFTSRK(2,3) satisfy these requirements. In addition, we verify that [74] some amplification functions of sIFTSRK go to zero as $\tau\kappa$ approaches $+\infty$, because of the exponential term $\mathrm{e}^{-(1+c_i)\tau\kappa}$. As an improvement, it can be seen that the amplification functions of the proposed pIFTSRK1/2 are equal to 1 from the proof of Theorem 3.1. Therefore, the pIFTSRK1/2 schemes not only promote the unconditionally MPP schemes to the eighth-order, but also remove the exponential decay/growth effects of traditional sIFTSRK schemes.

Remark 3.3. In addition to the preservation of the maximum principle using scheme pIFTSRK1/2, we point out that pTSRK1/2 with a suitable parameter κ also unconditionally preserve general inequality structures, such as the strong stability, positivity, range boundedness, and contractivity, when the right-hand-side term satisfies a forward Euler condition, as presented in Appendix A.

Remark 3.4. In the literature, some novel approximations of exponential functions in the integrating factor framework have been proposed. The approximations of pTSRK1/2 differ from those proposed by Huang *et al*. [38] and Du *et al*. [17] in several aspects. First, the conservative approximations [17] using Shu-Osher coefficients require additional order conditions on the Shu-Osher Runge-Kutta coefficients, while the pTSRK1 using Butcher coefficients retains the convergence characteristic without imposing other requirements. Second, in comparison with the approximations using Taylor expansions [38], the pTSRK2 schemes conserve linear invariants. Third, pTSRK1/2 preserve the inequality structures for any time-step size, in contrast to the strategies proposed in [17,38].

3.6 Second-order finite difference spatial discretization

For simplicity, we consider the interval (x_L,x_R) with periodic boundary conditions. Let the mesh size $h=(x_R-x_L)/N$. Denote the grid points as

$$\Omega_h = \{x_j \,|\, x_j = x_L + jh,\ j=0,1,\ldots,N-1\}.$$

Let

$$\mathbb{V}_N=\left\{\boldsymbol{v}\middle|\boldsymbol{v}=\left[v(x_0),\cdots,v(x_j),\cdots,v(x_{N-1})\right]^T,\ x_j\in\Omega_h\right\}\subset\mathbb{R}^N$$

be the space of grid functions defined on Ω_h, equipped with the l^2-inner product, and l^∞-norm defined as

$$\langle\boldsymbol{u},\boldsymbol{v}\rangle:=h\boldsymbol{v}^T\boldsymbol{u}=h\sum_{j=0}^{N-1}u_jv_j,\quad \|\boldsymbol{u}\|_{l^\infty}=\max_i|u_i|,\quad \forall\boldsymbol{u},\boldsymbol{v}\in\mathbb{V}_N.$$

Then, the induced ∞-norm of matrix is given by

$$\|A\boldsymbol{u}\|_\infty=\sup_{\|\boldsymbol{u}\|_{l^\infty}=1}\|A\boldsymbol{u}\|_{l^\infty},\quad \forall A\in\mathbb{R}^{N\times N},\quad \boldsymbol{u}\in\mathbb{R}^N.$$

Denote the central finite difference discretization of ∂_{xx} by

$$D_2=\frac{1}{h^2}\begin{bmatrix}-2&1&&&1\\1&-2&1&&\\&\vdots&\vdots&\vdots&\\&&1&-2&1\\1&&&1&-2\end{bmatrix}_{N\times N}.$$

Let $L=\epsilon^2D_2$ and $L_\kappa=\epsilon^2D_2-\kappa I$, where $I\in\mathbb{R}^{N\times N}$ is the identity matrix. The following lemmas hold.

Lemma 3.2 ([75]). *For any $\kappa\geq0$ and $\tau>0$, it holds that $\|\mathrm{e}^{\tau L_\kappa}\|_\infty=\mathrm{e}^{-\tau\kappa}\leq1$.*

Lemma 3.3 ([75]). *For any $\kappa\geq0$ and $\tau>0$, by letting $\mathbf{1}=[1,1,\cdots,1]^T\in\mathbb{R}^N$, it holds that $\langle\mathrm{e}^{\tau L_\kappa}\boldsymbol{u}^n,\mathbf{1}\rangle=\mathrm{e}^{-\tau\kappa}\langle\boldsymbol{u}^n,\mathbf{1}\rangle,\forall\kappa\geq0,\tau>0$.*

By applying pIFTSRK1/2 in the temporal direction and the second-order finite difference method in the spatial discretization, we obtain pIFTSRK1 (FD)

$$\begin{aligned}\boldsymbol{u}_{n,i}&=\sum_{j=-1}^{0}\hat{d}_{i,j}\mathrm{e}^{(c_i-c_j)\tau L}\boldsymbol{u}_{n,j}+\tau\sum_{j=-1}^{i-1}\hat{a}_{i,j}\mathrm{e}^{(c_i-c_j)\tau L}N(\boldsymbol{u}_{n,j})\\&=\frac{1}{\psi_i(\tau\kappa)}\left[\sum_{j=-1}^{0}d_{i,j}\mathrm{e}^{(1+c_j)\tau\kappa}\mathrm{e}^{(c_i-c_j)\tau L}\boldsymbol{u}_{n,j}+\tau\sum_{j=-1}^{i-1}a_{i,j}\mathrm{e}^{(1+c_j)\tau\kappa}\mathrm{e}^{(c_i-c_j)\tau L}N_\kappa(\boldsymbol{u}_{n,j})\right],\\&i=1,\ldots,s,\end{aligned}\tag{3.24}$$

and pIFTSRK2 (FD)

$$\begin{aligned}\boldsymbol{u}_{n,i}&=\frac{1}{\psi_i(\tau\kappa)}\left[\sum_{j=-1}^{0}d_{i,j}\psi_j(\tau\kappa)\mathrm{e}^{(c_i-c_j)\tau L}\boldsymbol{u}_{n,j}+\tau\sum_{j=-1}^{i-1}a_{i,j}\psi_j(\tau\kappa)\mathrm{e}^{(c_i-c_j)\tau L}N_\kappa(\boldsymbol{u}_{n,j})\right],\\&i=1,\ldots,s.\end{aligned}\tag{3.25}$$

Here, $N(\boldsymbol{u})$ denotes the spatial discretization of the nonlinear term $\mathcal{N}(u)$. For the RSLM formulation, the Lagrange multiplier appearing in the nonlinear term is computed by $\lambda(t)=\langle f(\boldsymbol{u}),\mathbf{1}\rangle/|\Omega|$.

We show that under certain requirements of the TSRK Butcher tableau (3.2) and κ, pIFTSRK1/2 (FD) preserve the maximum principle and conserve the mass of (2.1) unconditionally.

Theorem 3.3. *Assume that κ satisfies condition* (2.6) *and the underlying* TSRK *Butcher tableau of* pIFTSRK1/2 *satisfies Assumption* 3.1. *Then, if the starting values satisfy $\|\boldsymbol{u}^j\|_{l^\infty}\leq\beta, j=0,1$, the solutions obtained from the* pIFTSRK1/2 (FD) (3.24)/(3.25) *always satisfy $\|\boldsymbol{u}^{n+1}\|_{l^\infty}\leq\beta$ for any $\tau>0$.*

Proof. Consider the pIFTSRK2 (3.25) as an example. We prove this by mathematical induction. Assuming that $\|\boldsymbol{u}_{n,j}\|_{l^\infty}\leq\beta, j=-1,0,\ldots,i-1$, by applying Lemmas 2.4, 3.2, and the definitions of $\psi_i(\tau\kappa)$, we obtain

$$\begin{aligned}\|\boldsymbol{u}_{n,i}\|_{l^\infty}&\leq\frac{1}{\psi_i(\tau\kappa)}\left[\sum_{j=-1}^{0}d_{i,j}\psi_j(\tau\kappa)\left\|\mathrm{e}^{(c_i-c_j)\tau L}\boldsymbol{u}_{n,j}\right\|_{l^\infty}+\tau\sum_{j=-1}^{i-1}a_{i,j}\psi_j(\tau\kappa)\left\|\mathrm{e}^{(c_i-c_j)\tau L}N_\kappa(\boldsymbol{u}_{n,j})\right\|_{l^\infty}\right]\\&\leq\frac{1}{\psi_i(\tau\kappa)}\left[\sum_{j=-1}^{0}d_{i,j}\psi_j(\tau\kappa)+\tau\kappa\sum_{j=-1}^{i-1}a_{i,j}\psi_j(\tau\kappa)\right]\beta=\beta,\quad i\leq s.\end{aligned}$$

Then, we have $\|\boldsymbol{u}^{n+1}\|_{l^\infty}=\|\boldsymbol{u}_{n,s}\|_{l^\infty}\leq\beta$. □

Theorem 3.4. *Assume the underlying* TSRK *Butcher tableau of* pIFTSRK1/2 *satisfies Assumption* 3.1. *Let $M_h^n=\langle\boldsymbol{u}^n,\mathbf{1}\rangle$ denote the discrete mass. If the starting values satisfy $M_h^1=M_h^0$, then the* pIFTSRK1/2 (FD) (3.24)/(3.25) *conserve the mass of the* RSLM *formulation* (1.2), *i.e.,*

$$M_h^{n+1}=M_h^0,\quad\forall\tau>0. \tag{3.26}$$

By using Lemma 3.3, the proof of Theorem 3.4 can be carried out in a similar manner to that of Theorem 3.2. Therefore, we omit it.

3.7 Fourier pseudo-spectral spatial discretization

For the interval (x_L,x_R) with periodic boundary conditions, letting N be an even integer denoting the number of subintervals, we consider the interpolation space $S_N=\mathrm{span}\{h_j(x),j=0,1,\ldots,N-1\}$, where $h_j(x)$ are trigonometric functions of degree $N/2$ given by [25,59]

$$h_j(x)=\frac{1}{N}\sum_{l=-N/2}^{N/2}\frac{1}{c_l}\mathrm{e}^{\mathrm{i}l\mu(x-x_j)}$$

with $c_l=1$ $(|l|\neq N/2)$, $c_{-N/2}=c_{N/2}=2$, $\mu=2\pi/(x_R-x_L)$.

Defining the interpolation operator $I_N: C(\Omega)\to S_N$,

$$I_N u(x)=\sum_{j=0}^{N-1} u(x_j)h_j(x),$$

and taking the second-order derivative, we obtain

$$\frac{\partial^2 I_N u(x_i)}{\partial x^2}=\sum_{j=0}^{N-1} u(x_j)h_j^{(2)}(x_i)=\sum_{j=0}^{N-1}(\bar{D}_2)_{i,j}u(x_j),$$

where $\bar{D}_2=[\bar{d}_{i,j}]\in\mathbb{R}^{N\times N}$ is the second-order Fourier differentiation matrix determined by

$$\bar{d}_{i,j}=\begin{cases}\dfrac{1}{2}\mu^2(-1)^{i+j+1}\sin^{-2}\left(\dfrac{(j-i)\pi}{N}\right), & i\neq j,\\ -\mu^2\dfrac{N^2+2}{12}, & i=j,\end{cases}\quad \text{for}\quad i,j=0,1,\ldots,N-1. \tag{3.27}$$

Noting that zero is an eigenvalue of $\bar{D}_2$ [64], letting $\bar{L}_\kappa=\epsilon^2\bar{D}_2-\kappa I$, we have the following lemma.

Lemma 3.4. *For any $\kappa\geq 0$ and $\tau>0$, it holds that*

$$\left\langle \mathrm{e}^{\tau\bar{L}_\kappa}\boldsymbol{u}^n,\mathbf{1}\right\rangle=\mathrm{e}^{-\tau\kappa}\langle\boldsymbol{u}^n,\mathbf{1}\rangle,\quad \forall\kappa\geq 0,\quad \tau>0.$$

Proof. Because $\mathbf{1}=[1,1,\cdots,1]^T\in\mathbb{R}^N$ is an eigenvector of $\epsilon^2\bar{D}_2-\kappa I$ corresponding to the eigenvalue $-\kappa$, the row sum of $\mathrm{e}^{\tau\bar{L}_\kappa}$ can be calculated by

$$\mathrm{e}^{\tau\bar{L}_\kappa}\mathbf{1}=\sum_{k=0}^{\infty}\frac{\tau^k}{k!}\left(\epsilon^2\bar{D}_2-\kappa I\right)^k\mathbf{1}=\sum_{k=0}^{\infty}\frac{\tau^k}{k!}\underbrace{\left(\epsilon^2\bar{D}_2-\kappa I\right)^k\mathbf{1}}_{=(-\kappa)^k\mathbf{1}}=\sum_{k=0}^{\infty}\frac{(-\tau\kappa)^k}{k!}\mathbf{1}=\mathrm{e}^{-\tau\kappa}\mathbf{1}. \tag{3.28}$$

The symmetry of $\bar{D}_2$ implies that

$$\left\langle \mathrm{e}^{\tau\bar{L}_\kappa}\boldsymbol{u},\boldsymbol{v}\right\rangle=\left\langle \boldsymbol{u},\mathrm{e}^{\tau\bar{L}_\kappa}\boldsymbol{v}\right\rangle,\quad \forall\boldsymbol{u},\boldsymbol{v}\in\mathbb{R}^N,$$

and then

$$\left\langle \mathrm{e}^{\tau\bar{L}_\kappa}\boldsymbol{u}^n,\mathbf{1}\right\rangle=\left\langle \boldsymbol{u}^n,\mathrm{e}^{\tau\bar{L}_\kappa}\mathbf{1}\right\rangle=\langle\boldsymbol{u}^n,\mathrm{e}^{-\tau\kappa}\mathbf{1}\rangle=\mathrm{e}^{-\tau\kappa}\langle\boldsymbol{u}^n,\mathbf{1}\rangle.$$

This completes the proof. □

Applying pIFTSRK1/2 and the Fourier pseudo-spectral discretization to (2.1) gives

$$\begin{aligned}&\text{pIFTSRK1/2 (FP):}\quad \boldsymbol{u}_{n,i}=\sum_{j=-1}^{0}\hat{d}_{i,j}\mathrm{e}^{(c_i-c_j)\tau\bar{L}}\boldsymbol{u}_{n,j}+\tau\sum_{j=-1}^{i-1}\hat{a}_{i,j}\mathrm{e}^{(c_i-c_j)\tau\bar{L}}N(\boldsymbol{u}_{n,j}),\\ &i=1,\ldots,s.\end{aligned} \tag{3.29}$$

Similar to Theorem 3.4, we present the mass conservation for the fully discrete system (3.29) without proof.

Theorem 3.5. *Assume the underlying* TSRK *Butcher tableau of* pIFTSRK1/2 *satisfies Assumption* 3.1. *Let* $M_h^n = \langle \boldsymbol{u}^n, \mathbf{1} \rangle$ *denote the discrete mass. If starting values satisfy* $M_h^1 = M_h^0$, *then the* pIFTSRK1/2 (FP) (3.29) *conserves the mass of the* RSLM *formulation* (1.2), *i.e.,* $M_h^{n+1} = M_h^0, \forall \tau > 0$.

Different from the second-order finite difference discretization, the matrix $\bar{D}_2$ (3.27) is not a diagonally dominant matrix. Thus the Fourier pseudo-spectral method does not inherit the contraction semi-group property of the Laplace operator as in Lemmas 2.2 and 3.2, and it cannot strictly preserve the maximum principle of the continuous equation. For example, letting $(x_L, x_R) = (0,2)$, we show the infinity norms of $e^{\tau \bar{L}}$ for different values of τ and N in Fig. 1. Clearly, since $\bar{D}_2$ is an approximation to the Laplace operator, and can be arbitrarily accurate in space, the values of $\|e^{\tau \bar{L}}\|_\infty$ are close to but not bounded by one. Nevertheless, Li [50] proved that the Fourier spectral and pseudo-spectral discretizations admit effective maximum principles that allow the numerical solution of the AC equation with the Ginzburg-Landau potential to deviate from the sharp bound by a controllable discretization error. In the numerical experiments, we will study the performance of uniformly high-order-accurate schemes by incorporating the pIFTSRK integrators with the FP discretization. For a strict derivation of the effective maximum principle using FP discretization, we refer to [50, Theorem 1.6].

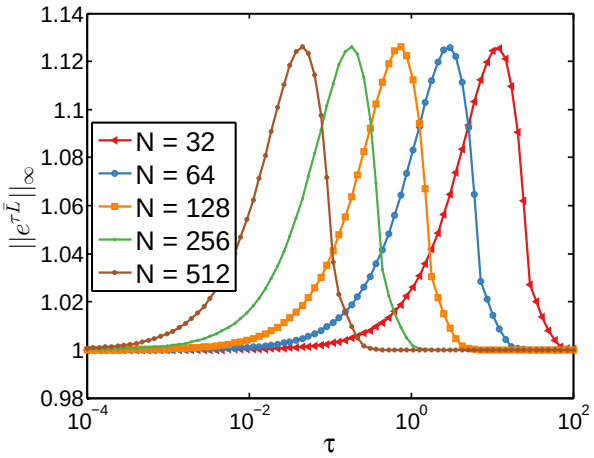

Figure 1: Infinity-norms of $e^{\tau \bar{L}}$ for different values of τ and N.

Remark 3.5. One advantage of using the proposed pIFTSRK schemes over the existing pIFRK schemes developed in [77] is that the pIFTSRK can promote the temporal convergence of unconditionally MPP schemes to the eighth-order, thus greatly reducing the splitting errors and time delay caused by stabilization techniques [70]. Moreover, to match the high-order spatial discretization of Fourier spectral Galerkin or collocation methods for the AC-type equation, it is also meaningful to develop high-order temporal integrators.

4 Numerical analysis

4.1 Stability regions

To obtain the stability regions of the proposed schemes, we consider the model equation [14]

$$u_t = -\kappa u + \lambda u, \tag{4.1}$$

where κ and λ are scalars. Applying pTSRK1 gives

$$u_{n,i} = \frac{1}{\psi_i(\tau\kappa)}\left[\sum_{j=-1}^{0} d_{i,j}\mathrm{e}^{(1+c_j)\tau\kappa}u_{n,j} + \tau\lambda\sum_{j=-1}^{i-1} a_{i,j}\mathrm{e}^{(1+c_j)\tau\kappa}u_{n,j}\right], \quad i=1,\ldots,s. \tag{4.2}$$

Letting

$$\Delta_i = \sum_{j=-1}^{0} d_{i,j}\mathrm{e}^{(1+c_j)\tau\kappa}u_{n,j}, \quad i=1,\ldots,s,$$

we reformulate (4.2) in the matrix form

$$(I-\tau\lambda\bar{A})\bar{u} = \bar{b}, \tag{4.3}$$

where

$$\begin{aligned}
&\bar{u} = [u_{n,-1}, u_{n,0}, \cdots, u_{n,s}]^T,\\
&[\bar{A}_{i+2,j+2}] = \left[a_{i,j}\frac{\mathrm{e}^{(1+c_j)\tau\kappa}}{\psi_i(\tau\kappa)}\right] \in \mathbb{R}^{(s+2)\times(s+2)}, \quad i,j=-1,\ldots,s,\\
&\bar{b} = \left[u_{n,-1}, u_{n,0}, \frac{\Delta_1}{\psi_1(\tau\kappa)}, \cdots, \frac{\Delta_s}{\psi_s(\tau\kappa)}\right]^T,
\end{aligned}$$

and $I \in \mathbb{R}^{(s+2)\times(s+2)}$.

Because the matrix $\bar{A}$ is strictly lower triangular, we can calculate that

$$u^{n+1} = S(\tau\kappa,\tau\lambda)[s+2], \tag{4.4}$$

where

$$S(\tau\kappa,\tau\lambda) = \sum_{k=0}^{s}(\tau\lambda)^k\bar{A}^k\bar{b} \in \mathbb{R}^{s+2}$$

and $[s+2]$ denotes the $(s+2)$-th entry of the vector $S(\tau\kappa,\tau\lambda)$.

The stability functions $S(\tau\kappa,\tau\lambda)$ for the classical IFTSRK and pTSRK2 can be obtained similarly. Letting $u^n = u^{n-1} = 1$ and requiring $|S(\tau\kappa,\tau\lambda)[s+2]| = 1$, we present boundaries of the stability regions of some third- to fifth-order IFTSRK and pTSRK1/2 schemes for $\kappa\tau = 0,1,\ldots,5$ and $\lambda\tau \in \mathbb{C}$ in Fig. 2.

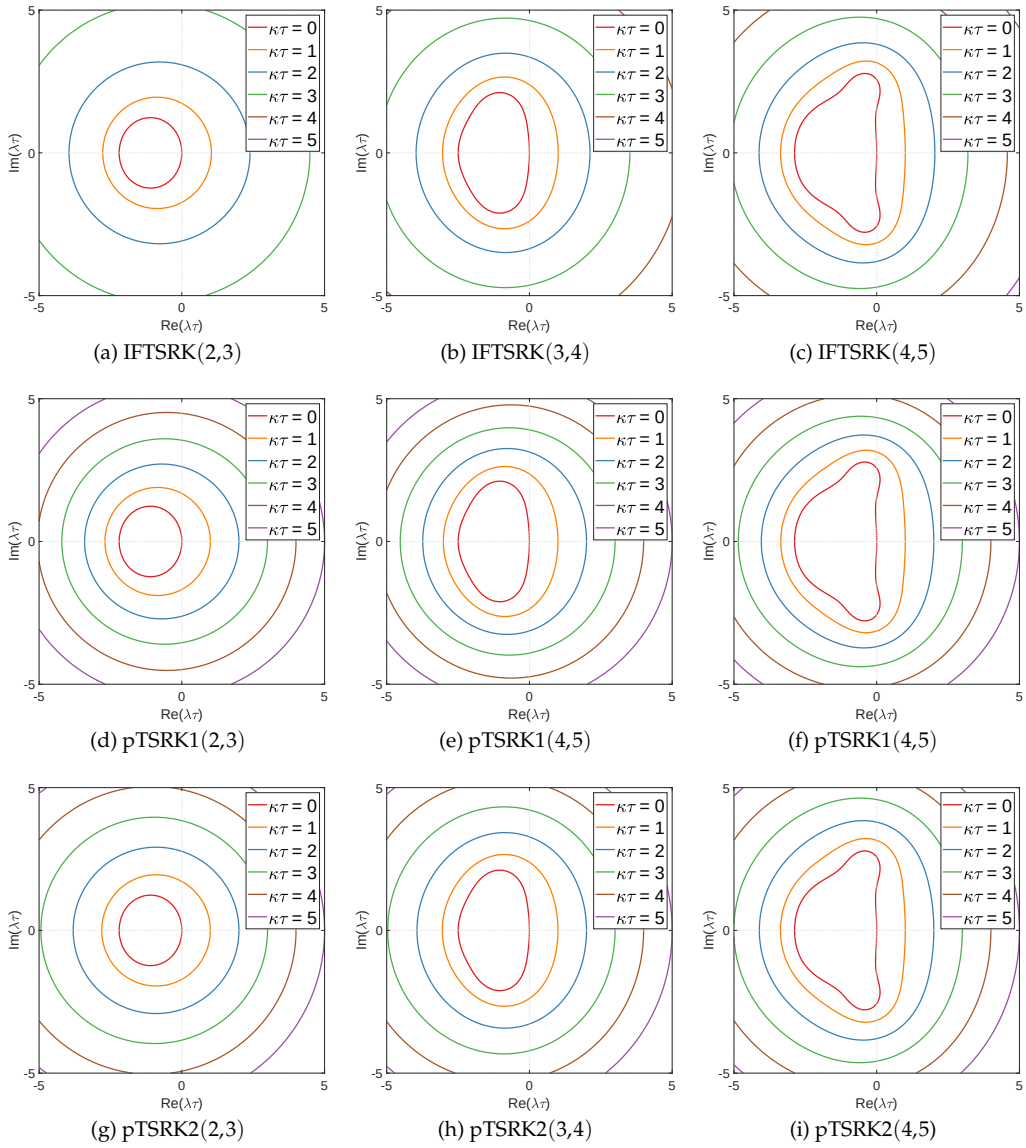

(a) IFTSRK(2,3) (b) IFTSRK(3,4) (c) IFTSRK(4,5)

(d) pTSRK1(2,3) (e) pTSRK1(4,5) (f) pTSRK1(4,5)

(g) pTSRK2(2,3) (h) pTSRK2(3,4) (i) pTSRK2(4,5)

Figure 2: Stability regions of IFTSRK, pTSRK1 and pTSRK2 with underlying TSRK(s, p) Butcher tableau.

From Fig. 2, we clearly see that for each scheme, the stability region monotonically becomes larger with the increasing $\kappa\tau$. Thus, the boundaries of stability regions obtained with $\kappa\tau = 4$ and 5 are not displayed in Fig. 2 (a). As a byproduct of eliminating the exponential effect, the stability regions become smaller for pTSRK1 and pTSRK2 when $\kappa\tau > 0$. We can also observe that the pTSRK2 schemes have larger stability regions than the pTSRK1 schemes. Furthermore, the IFTSRK and pTSRK1/2 methods reduce to the classical TSRK schemes when $\kappa\tau$ equals zero.

4.2 Convergence analysis

Using Theorem 3.1, and the truncation errors of the p-th order pTSRK1/2 schemes, we derive the following convergence result.

Theorem 4.1. *Assume that $u(t,x)\in C^{p+1}([0,T];C^2(\bar{\Omega}))$ is the exact solution to* (2.1) *and u^{n+1} is computed by the* pIFTSRK1/2 *scheme. For the underlying Butcher tableau provided in* [40] *satisfying Assumption* 3.1*, if the initial values are smooth and satisfy $\|u^i\|_{L^\infty}\leq\beta, i=0,1$, then we have following error estimate for the* pIFTSRK1/2 (3.21)/(3.22) *with the p-th order underlying Butcher tableau as*

$$\|u(t_{n+1})-u^{n+1}\|_{L^\infty}\leq \mathrm{e}^{l\kappa s t_{n+1}}\max_{j=0,1}\|e^j\|_{L^\infty}+C(\mathrm{e}^{l\kappa s t_{n+1}}-1)\tau^p \quad \textit{for} \quad t_n\leq T,$$

where $e^j=u(t_j)-u^j$, the constant $C>0$ depends on the $C^{p+1}([0,T];C^2(\bar{\Omega}))$ norm of u, the $C^p[-\beta,\beta]$-norm of f, and the stage numbers s, κ, l, but it is independent of τ.

Proof. Consider the pIFTSRK1 method as an example. We introduce the reference functions [20] $U_{n,i}$, $-1\leq i\leq s$, with $U_{n,j}=u(t_{n+j})$, $j=-1,0$, and $U_{n,s}=u(t_{n+1})$ satisfying

$$\begin{aligned}
U_{n,i}=&\frac{1}{\psi_i(\tau\kappa)}\Bigg[\sum_{j=-1}^{0}d_{i,j}\mathrm{e}^{(1+c_j)\tau\kappa}\mathrm{e}^{(c_i-c_j)\tau\mathcal{L}}u(t_{n+j})\\
&\qquad+\tau\sum_{j=-1}^{i-1}a_{i,j}\mathrm{e}^{(1+c_j)\tau\kappa}\mathrm{e}^{(c_i-c_j)\tau\mathcal{L}}\mathcal{N}_\kappa(U_{n,j})\Bigg],\quad i=1,\dots,s-1,\\
U_{n,s}=&\frac{1}{\psi_s(\tau\kappa)}\Bigg[\sum_{j=-1}^{0}d_{s,j}\mathrm{e}^{(1+c_j)\tau\kappa}\mathrm{e}^{(1-c_j)\tau\mathcal{L}}u(t_{n+j})\\
&\qquad+\tau\sum_{j=-1}^{s-1}a_{s,j}\mathrm{e}^{(1+c_j)\tau\kappa}\mathrm{e}^{(1-c_j)\tau\mathcal{L}}\mathcal{N}_\kappa(U_{n,j})\Bigg]+R_s^n.
\end{aligned}\tag{4.5}$$

For an s-stage, p-th order pIFTSRK1 scheme, Corollary 3.1 shows that the truncation error satisfies

$$\max_{0\leq n\leq\lfloor T/\tau\rfloor-1}\|R_s^n\|_{L^\infty}\leq C_s\tau^{p+1},$$

where C_s depends on the $C^{p+1}([0,T];C^2(\bar{\Omega}))$-norm of u, $C^p[-\beta,\beta]$-norm of f, s and κ, but is independent of τ.

Let

$$e^{n+j}=u(t_{n+j})-u^{n+j},\quad e_{n,i}=U_{n,i}-u_{n,i},\quad -1\leq i\leq s,$$

then $e_{n,j}=e^{n+j}$, $j=-1,0$ and $e_{n,s}=e^{n+1}$. Subtracting (3.21) from (4.5) yields

$$e_{n,i}=\frac{1}{\psi_i(\tau\kappa)}\Bigg[\sum_{j=-1}^{0}d_{i,j}\mathrm{e}^{(1+c_j)\tau\kappa}\mathrm{e}^{(c_i-c_j)\tau\mathcal{L}}e_{n,j}$$

$$+\tau\sum_{j=-1}^{i-1}a_{i,j}\mathrm{e}^{(1+c_j)\tau\kappa}\mathrm{e}^{(c_i-c_j)\tau\mathcal{L}}\big(\mathcal{N}_\kappa(U_{n,j})-\mathcal{N}_\kappa(u_{n,j})\big)\Big],\quad i=1,\ldots,s-1,$$

$$e_{n,s}=\frac{1}{\psi_s(\tau\kappa)}\Big[\sum_{j=-1}^{0}d_{s,j}\mathrm{e}^{(1+c_j)\tau\kappa}\mathrm{e}^{(1-c_j)\tau\mathcal{L}}e_{n,j}$$
$$+\tau\sum_{j=-1}^{s-1}a_{s,j}\mathrm{e}^{(1+c_j)\tau\kappa}\mathrm{e}^{(1-c_j)\tau\mathcal{L}}\big(\mathcal{N}_\kappa(U_{n,j})-\mathcal{N}_\kappa(u_{n,j})\big)\Big]+R_s^n.$$

The MPP property guarantees that $\|u_{n,i}\|_{L^\infty}\le\beta$ and $\|U_{n,i}\|_{L^\infty}\le\beta,-1\le i\le s$. Accordingly, using Lemma 2.4, we obtain

$$\|\mathcal{N}_\kappa(U_{n,j})-\mathcal{N}_\kappa(u_{n,j})\|_{L^\infty}\le l\kappa\|e_{n,j}\|_{L^\infty}.$$

It can be verified that all of the non-negative and non-decreasing SSP TSRK schemes developed in [40] satisfy

$$0<\sum_{j=-1}^{0}a_{i,j}\le1,\quad 0<\frac{\mathrm{e}^{(1+c_j)\tau\kappa}}{\psi_i(\tau\kappa)}\le1,\quad i=1,\ldots,s,\quad j=-1,0,\ldots,i-1.$$

Together with

$$\sum_{j=-1}^{0}d_{i,j}=1,\quad \|\mathrm{e}^{(c_i-c_j)\tau\mathcal{L}}u\|_{L^\infty}\le\|u\|_{L^\infty},\quad \|\mathrm{e}^{(c_i-c_j)\tau\mathcal{L}}u\|_{L^\infty}\le\|u\|_{L^\infty},$$

we derive

$$\begin{aligned}\|e_{n,i}\|_{L^\infty}&\le\frac{1}{\psi_i(\tau\kappa)}\Big[\sum_{j=-1}^{0}d_{i,j}\mathrm{e}^{(1+c_j)\tau\kappa}\big\|\mathrm{e}^{(c_i-c_j)\tau\mathcal{L}}e_{n,j}\big\|_{L^\infty}\\&\qquad+\tau\sum_{j=-1}^{i-1}a_{i,j}\mathrm{e}^{(1+c_j)\tau\kappa}\big\|\mathrm{e}^{(c_i-c_j)\tau\mathcal{L}}(\mathcal{N}_\kappa(U_{n,j})-\mathcal{N}_\kappa(u_{n,j}))\big\|_{L^\infty}\Big]\\&\le\max_{j=-1,0}\|e_{n,j}\|_{L^\infty}+l\tau\kappa\sum_{j=-1}^{i-1}a_{i,j}\|e_{n,j}\|_{L^\infty}\\&\le(1+l\tau\kappa)\max_{j=-1,0}\|e_{n,j}\|_{L^\infty}+l\tau\kappa\sum_{j=1}^{i-1}\|e_{n,j}\|_{L^\infty}\\&\le(1+l\tau\kappa)^i\max_{j=-1,0}\|e_{n,j}\|_{L^\infty},\quad i=1,\ldots,s-1,\\\|e_{n,s}\|_{L^\infty}&\le\frac{1}{\psi_s(\tau\kappa)}\Big[\sum_{j=-1}^{0}d_{s,j}\mathrm{e}^{(1+c_j)\tau\kappa}\|\mathrm{e}^{(1-c_j)\tau\mathcal{L}}e_{n,j}\|_{L^\infty}\\&\qquad+\sum_{j=-1}^{s-1}a_{s,j}\tau\mathrm{e}^{(1+c_j)\tau\kappa}\big\|\mathrm{e}^{(1-c_j)\tau\mathcal{L}}\big(\mathcal{N}_\kappa(U_{n,j})-\mathcal{N}_\kappa(u_{n,j})\big)\big\|_{L^\infty}\Big]+\|R_s^n\|_{L^\infty}\end{aligned}$$

$$\leq (1+l\tau\kappa)\max_{j=-1,0}\|e_{n,j}\|_{L^\infty}+l\tau\kappa\sum_{j=1}^{s-1}\|e_{n,j}\|_{L^\infty}+C_s\tau^{p+1}$$
$$\leq (1+l\tau\kappa)^s\max_{j=-1,0}\|e_{n,j}\|_{L^\infty}+C_s\tau^{p+1}.$$

By induction, we obtain

$$\|e^{n+1}\|_{L^\infty}\leq (1+l\tau\kappa)^{sn}\max_{j=-1,0}\|e^{1+j}\|_{L^\infty}+C_s\tau^{p+1}\sum_{i=0}^{n-1}(1+l\tau\kappa)^{si}$$
$$\leq \mathrm{e}^{l\kappa sn\tau}\max_{j=0,1}\|e^j\|_{L^\infty}+\frac{C_s}{l\kappa s}(\mathrm{e}^{l\kappa sn\tau}-1)\tau^p.$$

Letting $C=C_s/(l\kappa s)$, we obtain the desired result, since $t_{n+1}>n\tau$. The convergence of the pIFTSRK2 can be proven similarly. □

5 Numerical experiments

In this section, we present numerical experiments to demonstrate the effectiveness and inequality-preserving properties of the proposed schemes. All the TSRK Butcher tableaux used in this work were downloaded from the repository [27]. If not specified, the maximum bounds for the pSG equation and RSLM formulation were chosen to be $\beta=\pi$ and $\beta=3\pi/2$, respectively. In the simulations, we computed products of the matrix exponentials with vectors via the fast Fourier transform to accelerate the computations [18].

5.1 Convergence tests

Example 5.1. We first tested the stability and accuracy of the proposed integrators on a stiff nonlinear benchmark system of ordinary differential equations (ODEs) from [72],

$$\begin{cases} u_t=\dfrac{u-cv^7}{2\sqrt{v}}-\dfrac{1}{2}, \\ v_t=u-\sqrt{v}-cv^7 \end{cases} \tag{5.1}$$

with initial values $u^0=1.0$, $v^0=1.0$, where c is a parameter that determines the stiffness of the problem. This system has an exaction solution

$$u(t)=(6ct+1)^{-\frac{1}{12}},\quad v(t)=(6ct+1)^{-\frac{1}{6}}.$$

For comparison, we considered different stiffness by setting $c=10,100,1000$, and solved this problem to time $t=0.1$ using the existing ETD2 [18] (Appendix B), pRK2(4,4) [77] (Appendix B), TSRK(4,5) [40], and the proposed fourth- to eighth-order pTSRK1/2 schemes. The corresponding stabilization parameters for the schemes ETD2, pRK2(4,4),

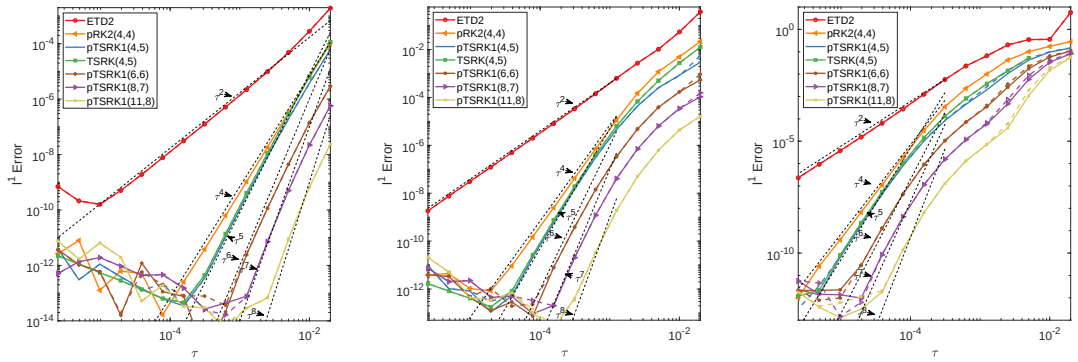

(a) $\kappa=c=10$ (b) $\kappa=c=100$ (c) $\kappa=c=1000$

Figure 3: Example 5.1. Time accuracy tests of ETD2, pRK2$(4,4)$, TSRK$(4,5)$, pTSRK1/2 for Eq. (5.1) at $t=0.1$. Colored dashed curves denote errors obtained using pTSRK2 (some overlap with those of pTSRK1).

and pTSRK1/2, were chosen as $\kappa=c$. Numerical errors in the l^1-norm are presented in Fig. 3. When the stiffness of the system was not strong ($c=10$), we can observe the expected convergence orders of the ETD2, pRK2$(4,4)$, TSRK$(4,5)$, and pTSRK1/2 schemes. Since the pTSRK1/2$(4,5)$ utilized two-step solutions, the numerical errors were significantly smaller than those of the ETD2, and the convergence rate was one order higher than the pRK2$(4,4)$. This demonstrates the advantages of using two-step high-order methods. Upon increasing c to 1000, the TSRK$(4,5)$ integrator (green square curve) blew up at large time steps, so the errors were not plotted in Fig. 3 (c). Since ETD2, pRK2$(4,4)$, and pTSRK1/2 require large stabilization parameters to ensure the stability, the corresponding errors in Figs. 3 (b,c) were higher than those in Fig. 3 (a). Thus, the convergence orders were reduced at large time steps, which is common phenomenon of stabilization methods [17,72].

Example 5.2. We then tested the temporal and spatial convergence of the proposed schemes on the 1D pSG Eq. (1.1) and its RSLM reformulation (1.2) with periodic boundary conditions and the smooth initial value

$$u(x,t=0)=0.1\sin(2\pi x)+0.05,\quad x\in(0,2),\quad t>0. \tag{5.2}$$

We set $\epsilon=0.01$ and solved this problem to time $T=4.0$. The numerical errors were computed using

$$\text{Error}_{l^\infty}=\|\bar{\boldsymbol{u}}^n-\boldsymbol{u}^n\|_{l^\infty},$$

where $\bar{\boldsymbol{u}}^n$ is the reference solution computed with a refined step size and $\boldsymbol{u}^n$ is the numerical solution. For the temporal convergence, the grid number was set to be $N=2^8$ and the reference solution was computed with $\tau=2^{-12}$ using the eighth-order IFTSRK(11, 8) (FD). The starting values for two-step schemes were found using the fourth-order unconditionally MPP parametric IFRK scheme proposed in [77] with a refined time-step size. We set the stabilization parameter $\kappa=1$ for both stabilized formulations.

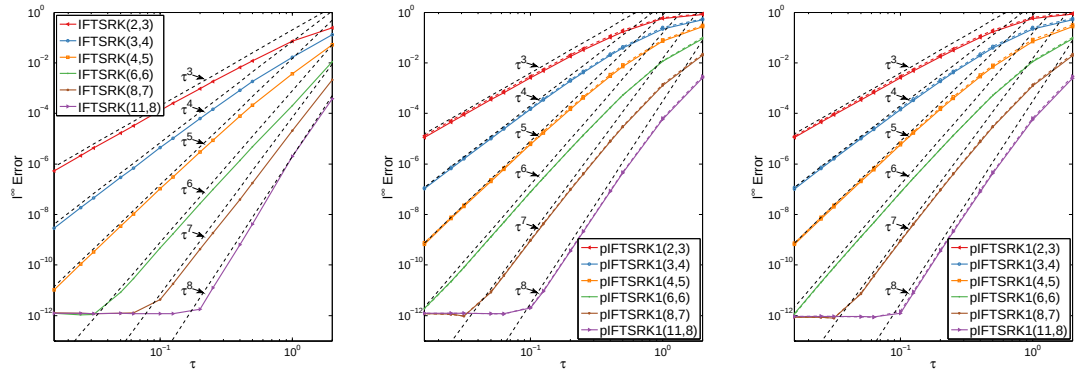

(a) IFTSRK, Eq. (1.1), $\kappa=0$ (b) pIFTSRK1/2, Eq. (1.1), $\kappa=1$ (c) pIFTSRK1/2, Eq. (1.2), $\kappa=1$

Figure 4: Example 5.2. Time accuracy tests of IFTSRK (FD) and pIFTSRK1/2 (FD) at $T=4$. The reference slopes in (b) and (c) are fixed. The colored dashed curves in (b) and (c) denote the errors obtained using pIFTSRK2 (FD) (some overlap with those of pIFTSRK1).

The results of the numerical convergence study at $T=4$ obtained by the IFTSRK (FD) and the proposed pIFTSRK1/2 (FD) for the pSG equation and RSLM reformulation are shown in Fig. 4. Each of the third- to eighth-order schemes converged with the expected order of accuracy when applied to different models. The comparison of the sub-figures in Fig. 4 shows that the numerical errors of the IFTSRK were smaller than those of the pIFTSRK1 and pIFTSRK2 because of the splitting errors introduced by the stabilization. Figs. 4 (b,c) demonstrate that the accuracy of the pIFTSRK2 schemes was very close to that of the pIFTSRK1. In addition, with the introduction of $\kappa=1$, the introduced numerical errors clearly demonstrated the necessity of developing high-order-accurate schemes.

Next, we tested the spatial accuracy of the FD and FP for the RSLM formulation by choosing the moderate pIFTSRK1(4,5) as the temporal integrator, fixing the time step $\tau=2^{-10}$, and refining the spatial grid from $N=2^6$ to $N=2^9$ uniformly. The reference solution was computed with $N_{ref}=2^{12}$ and $\tau=2^{-10}$. As expected, the second-order convergence of the finite-difference discretization, and the spectral accuracy of the Fourier pseudo-spectral discretization were obtained, as shown in Table 1.

Table 1: Spatial accuracy tests of FD and FP discretizations for the RSLM formulation. Underlying temporal integrator: pIFTSRK1(4,5). Parameters: $\tau=2^{-10}$, $\kappa=1$, $T=4$, $N_{ref}=2^{12}$.

Scheme	N	l^∞ Error	Order	Scheme	l^∞ Error	Order
pIFTSRK1 (FD)	2^6	1.736e-3	-	pIFTSRK1 (FP)	3.409e-5	-
	2^7	4.559e-4	1.929		4.028e-8	9.725
	2^8	1.151e-4	1.986		4.743e-13	16.374
	2^9	2.882e-5	1.997		5.800e-13	-0.290

5.2 Structure-preserving tests

Example 5.3. We first demonstrate the positivity-preservation (Appendix A) of pTSRK by considering a benchmark stiff linear system of ODEs [37,41] with the form

$$\boldsymbol{u}_t = A\boldsymbol{u} = 100\begin{bmatrix} -2 & 1 & 1 \\ 1 & -4 & 1 \\ 1 & 3 & -2 \end{bmatrix}\boldsymbol{u}, \quad \boldsymbol{u}^0 = \begin{bmatrix} 1 \\ 9 \\ 5 \end{bmatrix}. \tag{5.3}$$

The exact solution reads

$$\boldsymbol{u}(t) = c_1\begin{bmatrix} 5 \\ 3 \\ 7 \end{bmatrix} + c_2\mathrm{e}^{-300t}\begin{bmatrix} -1 \\ 0 \\ 1 \end{bmatrix} + c_3\mathrm{e}^{-500t}\begin{bmatrix} 0 \\ -1 \\ 1 \end{bmatrix}$$

with coefficients $c_1 = 1$, $c_2 = 4$, $c_3 = -6$ determined by the initial condition. Since the coefficient matrix is a so-called Metzler matrix [41], which has only positive off-diagonal elements, this ensures that the solution components are positive for all times because of the positive initial values. In addition, the ODE system has a linear invariant $M(\boldsymbol{u}) = \boldsymbol{u}^T\mathbf{1}$.

This problem requires $\tau \le \tau_{FE} = 1/400$ to guarantee the forward Euler condition of positivity, that is,

$$\exists \tau_{FE} = \frac{1}{400} \quad \text{such that} \quad u + \tau A u \ge 0, \quad \forall u \ge 0, \quad \forall \tau \in (0, \tau_{FE}],$$

where the inequalities are element-wise. Thus, to guarantee the positivity of the solution, the circle condition requires $\kappa \ge 1/\tau_{FE} = 400$. Because the exact solution converges to the equilibrium state $\boldsymbol{u}^* = [5,3,7]^T$ very rapidly, and the exponential functions in pTSRK1 blow up for $\kappa = 400$ and large time steps, we only demonstrate the positivity and linear invariant conservation of pTSRK2 at times steps larger than τ_{FE}.

We set $\kappa = 400$ and solved this problem to $T = 0.06$ and $T = 100$ with time steps τ=0.006 and 5.0, respectively. We chose TSRK(4,5) with the SSP coefficient $\mathcal{C} \approx 0.8542$ [40] as the underlying scheme. The numerical solutions computed using TSRK(4,5) and pTSRK2(4,5) are presented in Fig. 5. As $\tau = 0.006 > \mathcal{C}\tau_{FE}$, the solution obtained by TSRK(4,5) in Fig. 5 (a) was not positivity-preserving. With the introduction of stabilization, pTSRK2(4,5) with $\tau = 0.006$ preserved the positivity and linear inequality, as shown in Fig. 5 (a), and the solution closely followed the exact solution. After increasing τ to 5.0, the solution of TSRK(4,5) blew up, and thus, it is not presented. In Fig. 5 (b), we compare the solution of pTSRK2(4,5) with the exact one. There were no oscillations in the solution profile, and pTSRK2(4,5) preserved the positivity, fixed point, and linear invariant $M(\boldsymbol{u})$.

Example 5.4. To test the properties of proposed schemes on the pSG equations, we consider the 1D initial profile in Example 5.2. Since Fig. 2 and Examples 5.1 and 5.2 demonstrated that the stability and accuracy of pIFTSRK1 and pIFTSRK2 were very similar,

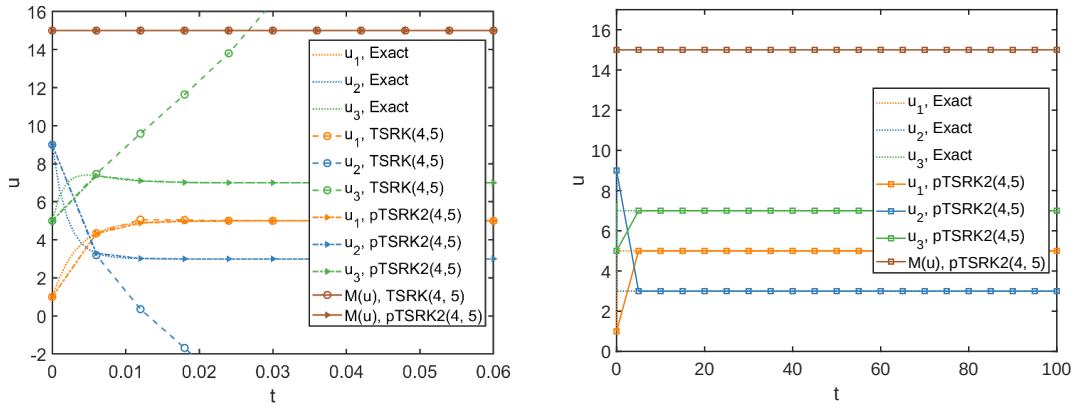

(a) Results of Eq.(5.3), $\tau=0.006$

(b) Results of Eq. (5.3), $\tau=5.0$

Figure 5: Example 5.3. Numerical solutions and linear invariants $M(\boldsymbol{u})$ obtained by different schemes with $\tau=0.006$ (a) and $\tau=5.0$ (b).

for comparison and simplicity, we solved the pSG equation and RSLM formulation using some fourth-, fifth- and eighth-order IFTSRK, and pIFTSRK1 schemes with $\epsilon=0.01$, $N=128$, and set the final time $T=100$.

Test 5.4 using FD. First, we tested the temporal integrators using the FD spatial discretization. Fig. 6 column (a) presents the results of the pSG equation computed with underlying TSRK(3,4) scheme. When the time step τ is increased from 0.1 to 2.5, IFTSRK(3,4) produced oscillations in the solution and energy profiles (first row and fourth row), and the maximum-principle was violated (second row). By introducing a stabilization term with $\kappa=1.0$, the solution computed with $\tau=2.5$ using the proposed pIFIFRK1 scheme, was not only accurate but also preserved the maximum principle, and dissipated the energy. When adopting the fifth-order underlying TSRK(4,5) scheme, although Fig. 6 column (b) shows that the solution computed using IFTSRK(4,5) with $\tau=4.0$ did not violate the maximum principle, the solution profile was no longer accurate (first row), and there were large differences between the energy profiles computed with $\tau=4.0$ and 0.1. With the introduction of $\kappa=1.0$, pIFTSRK(4,5) provided a very accurate solution, and well preserved such structures.

The results of the RSLM formulation computed by the highest eighth-order schemes are presented in column (c) of Fig. 6. Similar to the fourth-order scheme in column (a), the solution of IFTSRK with $\tau=7.0$ had oscillations. With suitable approximations of the exponential functions, the pIFTSRK1 scheme provided an accurate solution, preserved the maximum principle, conserved mass to machine accuracy, and dissipated the energy. In addition, there was little difference between the computed solution and the reference solution obtained.

Test 5.4 using FP. Next, we studied properties of the Fourier pseudo-spectral discretization using the moderate fifth-order and highest eighth-order pIFTSRK1 integra-

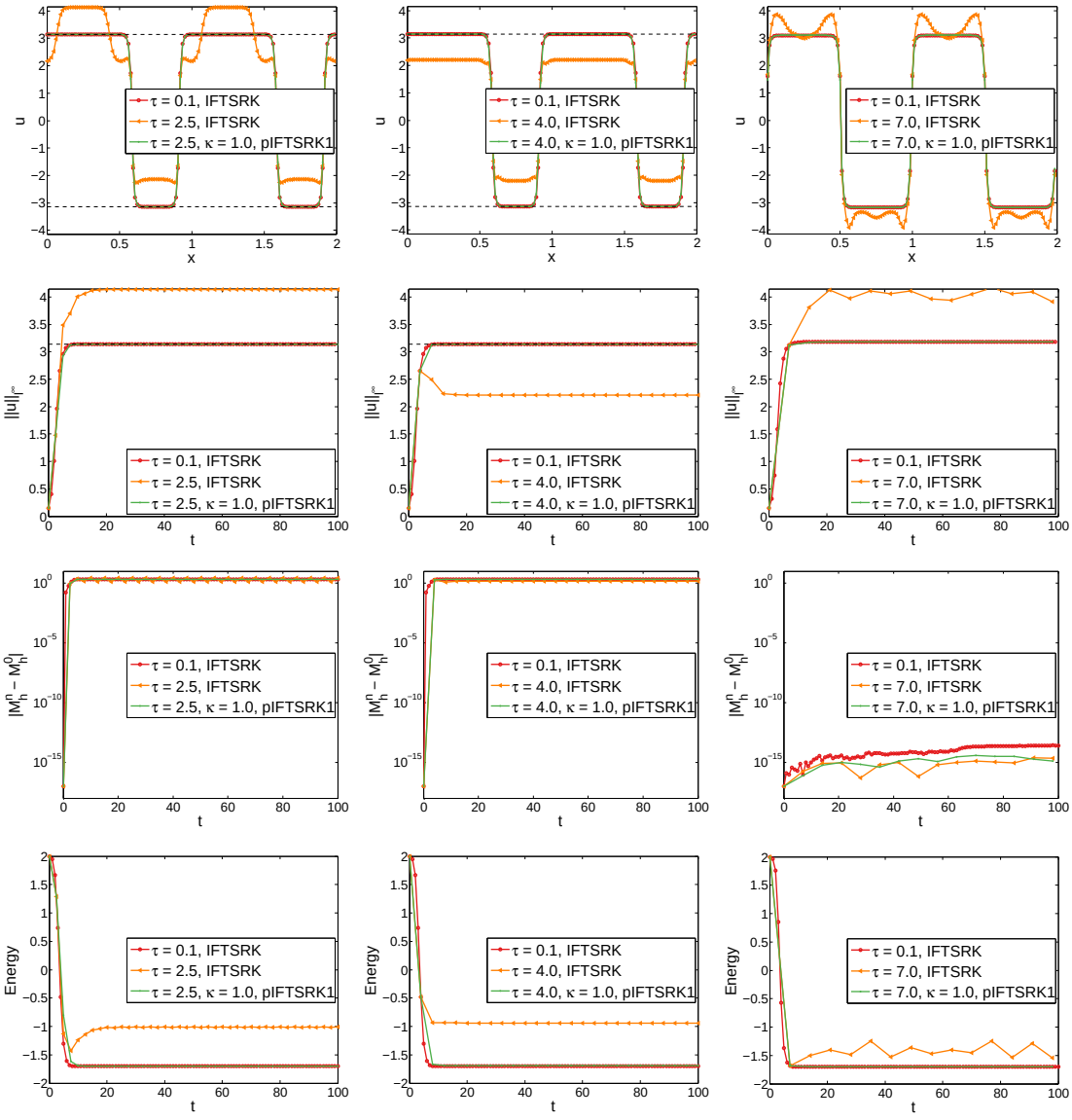

(a) TSRK(3, 4), pSG (b) TSRK(4, 5), pSG (c) TSRK(11, 8), RSLM

Figure 6: Test 5.4 (FD). The profiles of $\boldsymbol{u}$ (first row), evolutions of $\|\boldsymbol{u}\|_{l^\infty}$ (second row), absolute mass error $|M_h^n - M_h^0|$ (third row) and energy (fourth row) computed with different combinations of τ and κ using IFTSRK and pIFTSRK1. The black dashed lines in the first and second rows denote the levels of $\pm\pi$. Parameters: $\epsilon = 0.01$, $N = 128$.

tors. The largest values of $\{\|\boldsymbol{u}^n\|_{l^\infty}\}_{n=0,\ldots,N}$ for the pSG equation computed by schemes pIFTSRK1(4,5) and pIFTSRK1(11,8) with $\tau \in [10^{-2}, 10^2]$ and $N = 2^i, i = 5, \ldots, 9$ are presented in Fig. 7. Fig. 1 shows that the value of $\|e^{\tau L}\|_\infty$ was close to 1. It can be observed in Fig. 7 that, although the pIFTSRK1 (FP) integrators violated the maximum principle, they were

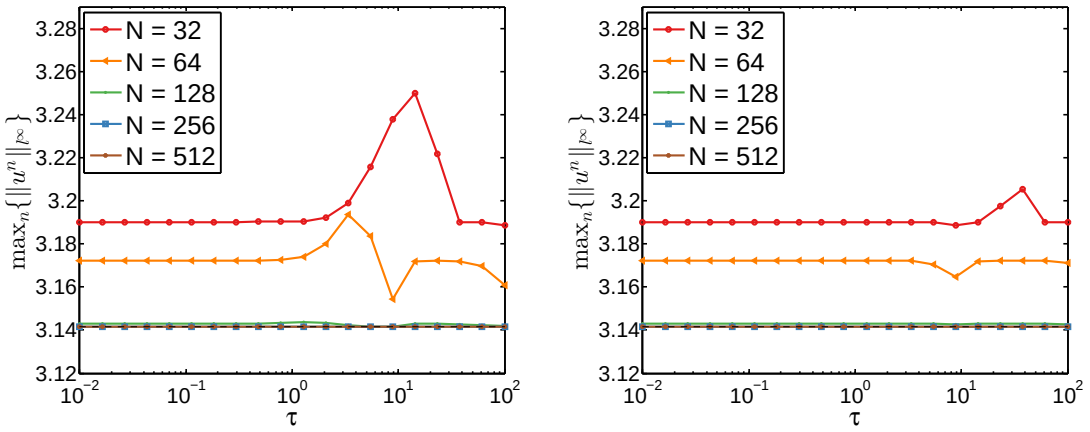

(a) pIFTSRK1(4,5) (b) pIFTSRK1(11,8)

Figure 7: Test 5.4 (FP). Plots of the largest values of $\{\|\boldsymbol{u}^n\|_{l^\infty}\}_{n=0,\ldots,N}$ for the pSG equation computed by pIFTSRK(4,5) (left) and pIFTSRK1(11,8) (right) with different values of τ and N. The black dashed lines denoting the level π overlap with the blue and brown curves. Parameters: $\epsilon=0.01$, $\kappa=1.0$, $T=100$.

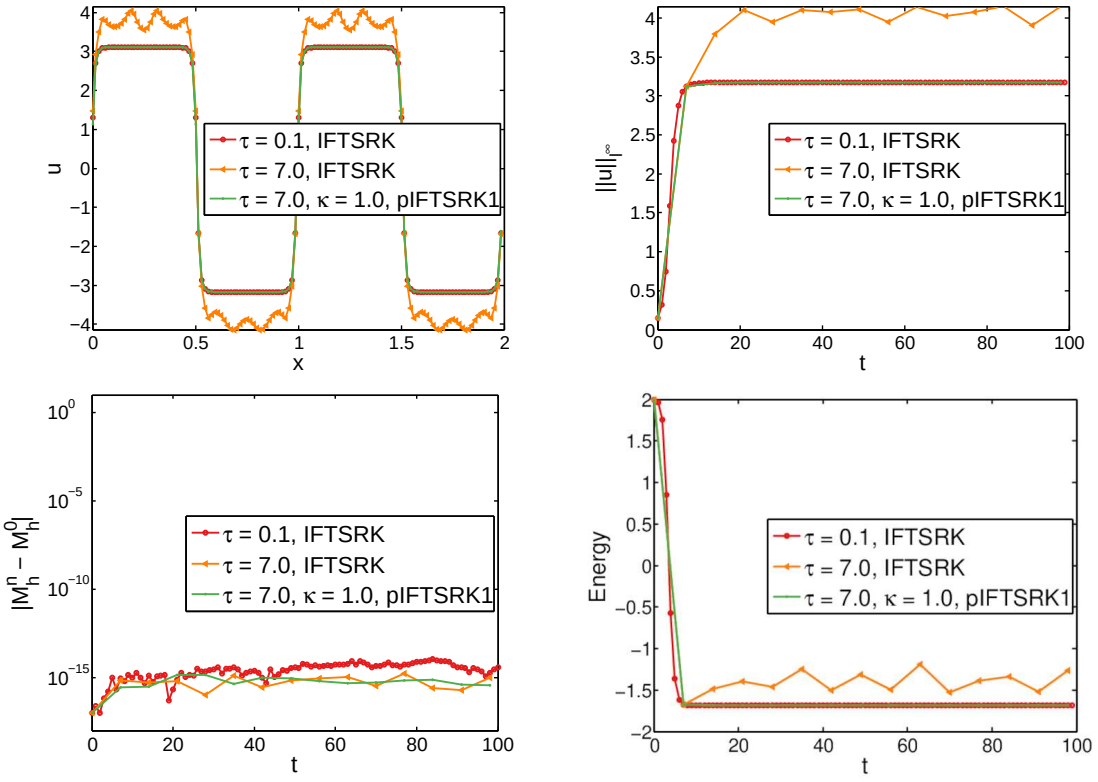

Figure 8: Test 5.4 (FP). Profiles of $\boldsymbol{u}$ (top left, t = 100), evolution of $\|\boldsymbol{u}\|_{l^\infty}$ (top right), absolute mass error $|M_h^n - M_h^0|$ (bottom left) and energy (bottom right) for the RSLM formulation computed with different τ and κ using IFTSRK(11,8) and pIFTSRK1(11,8). Parameters: $\epsilon=0.01$, $N=128$.

very stable, and the maximum bounds were close to the theoretical bound, especially when using a large grid number.

We present the results of the RSLM formulation computed by pIFTSRK1(11,8) (FP) with different values of τ and κ in Fig. 8. This shows that without stabilization, the IFTSRK with a large $\tau=7.0$ produced oscillations in the solution and finally violated the maximum principle and the energy dissipation law. With the introduction of $\kappa=1.0$, the proposed pIFTSRK1 made the solution stable and bounded. There was no difference in the eye-norm between the solution computed with $\tau=7.0$, $\kappa=1.0$ and the reference solution computed using IFTSRK with $\tau=0.1$. In addition, pIFTSRK1 conserved mass to machine accuracy and produced a very stable energy profile. Such behavior was very similar to that of pIFTSRK1 (FD) in Fig. 6 column (c).

Example 5.5. Consider the evolution of a 2D profile given by the three concave squares

$$u(x,y,t=0)=0.2\times\sum_{i=1}^{3}\tanh\left(100(0.25-|x-x_i|^{0.8}-|y-y_i|^{0.8})\right)+0.3,\quad (x,y)\in(-0.5,0.5)^2,$$

where $(x_i,y_i)\in\{(0,-0.15),(-0.2,0.15),(0.2,0.15)\}$.

The parameters were chosen as $\epsilon=0.01$, $N=128^2$. We solved the RSLM formulation using eighth-order schemes and the FD spatial discretization to the final time $T=500$. Fig. 9 presents the initial profile and the zero-level-set snapshots at $t=0,40,80,200,496$ computed by IFTSRK and pIFTSRK1. The 3D views of the solutions at t=40 are presented in Fig. 10, and the evolution of $\|\boldsymbol{u}\|_{l^\infty}$, the absolute mass error $|M_h^n-M_h^0|$, and the discrete energy are shown in Fig. 11.

For the IFTSRK scheme, we computed the reference solution using a refined time step $\tau=0.1$. Fig. 11 shows that the infinity-norm of the computed solution grew rapidly, but still satisfied the maximum principle. As time progressed, the three squares coalesced, and finally became circular, as shown in Fig. 9. When the time-step size was

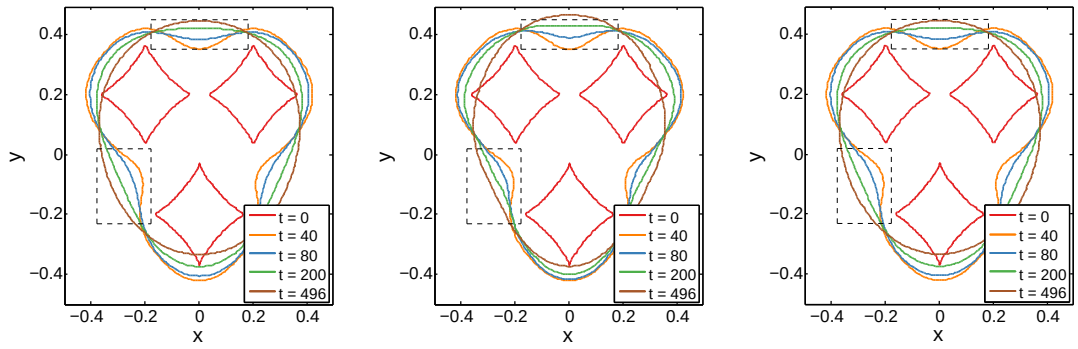

(a) $\tau=0.1$, IFTSRK(11,8) (b) $\tau=8.0$, IFTSRK(11,8) (c) $\tau=8.0$, $\kappa=1$, pIFTSRK1(11,8)

Figure 9: Example 5.5. Zero-level-set snapshots of the solutions of the RSLM computed by IFTSRK(11,8) and pIFTSRK(11,8) schemes. Parameters: $N=128^2$.

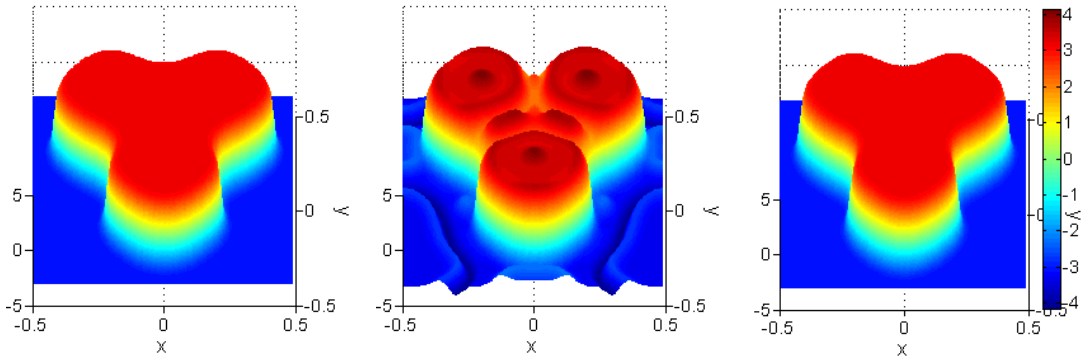

(a) $\tau=0.1$, IFTSRK$(11,8)$ (b) $\tau=8.0$, IFTSRK$(11,8)$ (c) $\tau=8.0$, $\kappa=1$, pIFTSRK1$(11,8)$

Figure 10: Example 5.5. 3D views of the solutions of the RSLM at $t=40$ computed by IFTSRK$(11,8)$ and pIFTSRK1$(11,8)$.

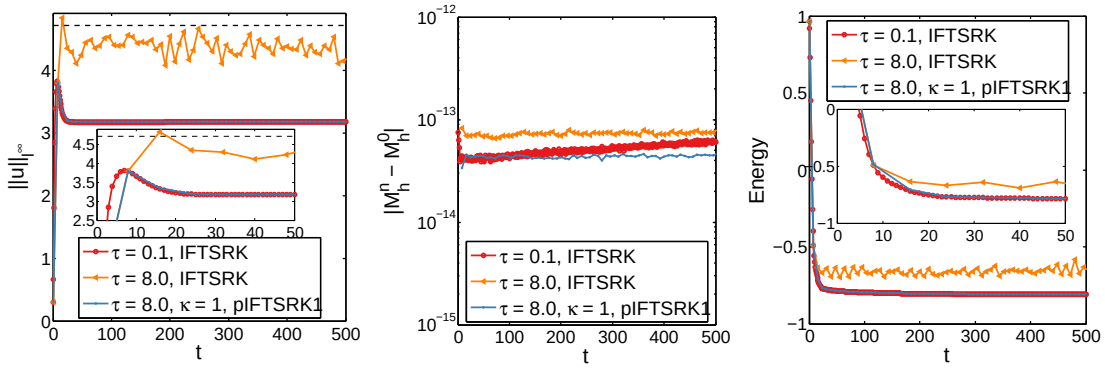

(a) $\|\boldsymbol{u}\|_{l^\infty}$ (b) $|M_h^n-M_h^0|$ (c) E_h

Figure 11: Example 5.5. Evolutions of $\|\boldsymbol{u}\|_{l^\infty}$ (a) absolute mass error $M_h^n-M_h^0$ (b) and energy E_h (c) of the RSLM formulation computed by IFTSRK$(11,8)$ and pIFTSRK1$(11,8)$. The black dashed line in (a) denotes the level of $3\pi/2$.

increased to $\tau=8.0$, the solution became unstable (Fig. 10 (b)), violated the maximum principle (Fig. 11 (a)), and the energy was no longer dissipative (Fig. 11 (c)). Again, when pIFTSRK1$(11,8)$ with $\tau=8.0,\kappa=1.0$ was applied, the computed solution was much better than that of the IFTSRK scheme. In Fig. 9, we can see that there are large differences between the outlines of the zero-level-set snapshots located in dashed rectangles computed by IFTSRK ($\tau=8.0$) in Fig. 9 (b) and the references curves in Fig. 9 (a), while the results obtained by pIFTSRK in Fig. 9 (c) were very close to the reference results. Fig. 10 (c) also demonstrates the increased accuracy of pIFTSRK when compared with those obtained by IFTSRK. In addition, Fig. 11 (blue curves in all sub-figures) clearly shows that pIFTSRK1$(11,8)$ well preserved the structures of the RSLM formulation.

The CPU time costs of IFTSRK and pIFTSRK1 are listed in Table 2. Because the pIFTSRK1 scheme with the stabilization parameter $\kappa=1$ allows a much larger time-step

Table 2: CPU time costs (s) for solving the RSLM formulation by the eighth-order IFTSRK and pIFTSRK1 with different values of τ and κ. Parameters: $T=500, N=128^2$.

Scheme	IFTSRK, $\tau=0.1$	IFTSRK, $\tau=8.0$	pIFTSRK, $\tau=8.0,\kappa=1.0$
CPU time (s)	380.92	5.38	5.29

size, the computational efficiency improved greatly without affecting the accuracy significantly.

Example 5.6. In this example, we consider the seven-circle benchmark problem [13,51] to demonstrate the similarity between the pSG equation and the AC equation ($u_t=\epsilon^2\Delta u+u-u^3$) with the Ginzburg-Landau potential. To make the results comparable, we perform a scaling and translation of the nonlinear potential function of the pSG, that is,

$$E(u)=\int_\Omega \frac{1}{2}\epsilon^2|\nabla u|^2+\frac{1}{\pi^2}\big(1+\cos(\pi u)\big)\mathrm{d}x.$$

Then, the pSG becomes

$$u_t=\epsilon^2\Delta u+\frac{1}{\pi}\sin(\pi u). \tag{5.4}$$

As a result, the maximum bound is replaced by $\beta=1$, which is same as that of the AC equation. The stabilization parameter κ of Eq. (5.4) remains the same, while the circle condition (2.2) requires $\kappa\geq 2.0$ for AC equation. The initial condition was chosen as

$$u(x,y,0)=-1+\sum_{i=1}^{u} f_0\Big(\sqrt{(x-x_i)^2+(y-y_i)^2}-r_i\Big),$$
$$\Omega=(0,2\pi)^2,\quad f_0(s)=\begin{cases}2\mathrm{e}^{-\epsilon^2/s^2}, & \text{if}\quad s<0,\\ 0, & \text{otherwise.}\end{cases}$$

The centers and radii of the seven circles are given in Table 3.

We chose the parameters ϵ=0.05, N=256^2, and solved the pSG (5.4) and AC equations using pIFTSRK1$(11,8)$ to the final time $T=200$ based on FD spatial discretization. The reference solutions for AC were computed using IFTSRK with $\tau=0.1$. Since the SSP coefficient of the underlying TSRK$(11,8)$ is $\mathcal{C}\approx 0.2743$ [40], we chose a critical time step

Table 3: Centers (x_i,y_i) and radii (r_i) of Example 5.6.

i	1	2	3	4	5	6	7
x_i	$\pi/2$	$\pi/4$	$\pi/2$	π	$3\pi/2$	π	$3\pi/2$
y_i	$\pi/2$	$3\pi/4$	$5\pi/4$	$\pi/4$	$\pi/4$	π	$3\pi/2$
r_i	$\pi/5$	$2\pi/15$	$2\pi/15$	$\pi/10$	$\pi/10$	$\pi/4$	$\pi/4$

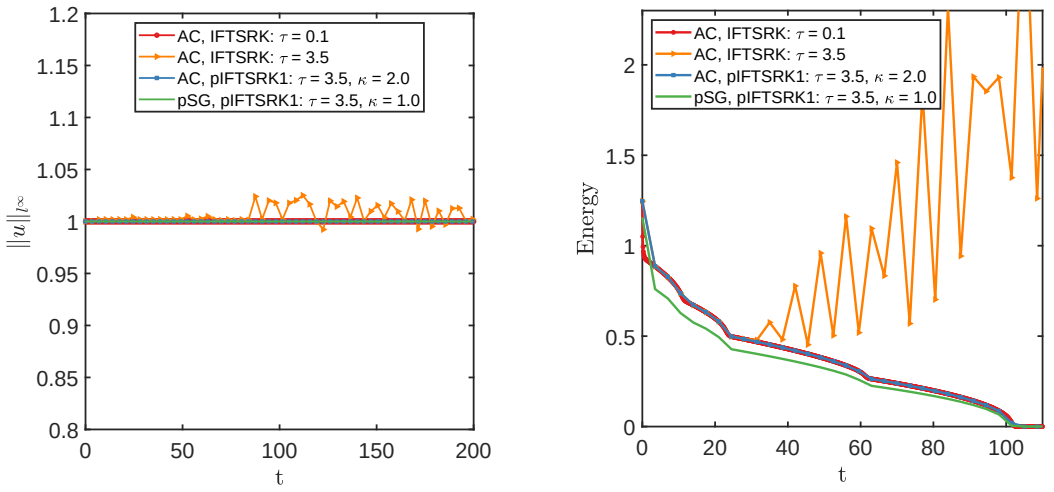

Figure 12: Example 5.6. Evolutions of maximum bounds and energy for AC and pSG.

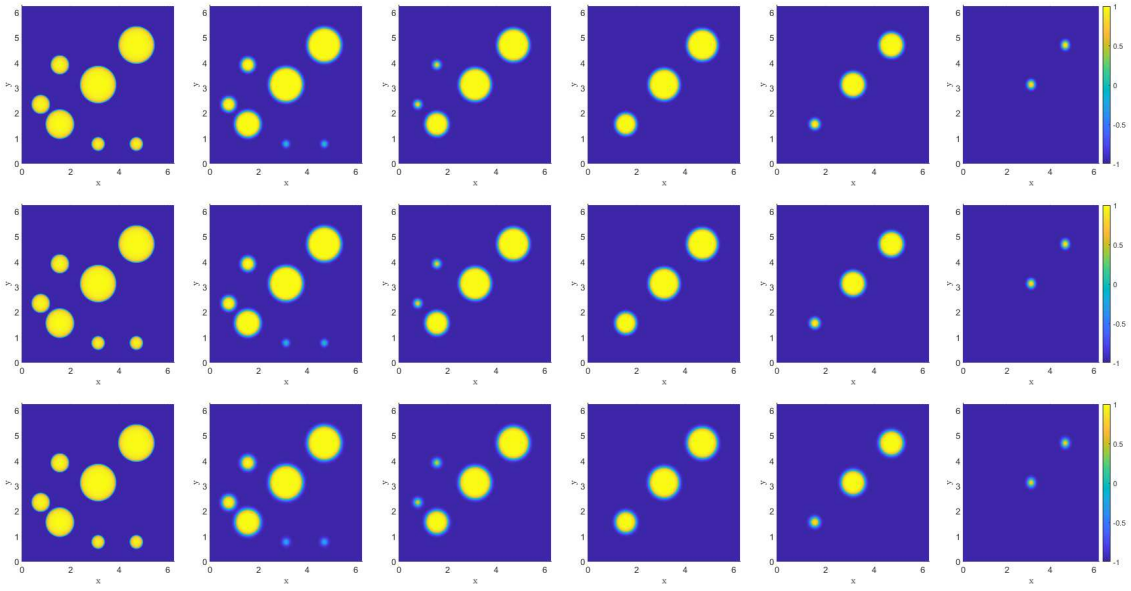

(a) $t=0.0$ (b) $t=10.5$ (c) $t=21.0$ (d) $t=28.0$ (e) $t=56.0$ (f) $t=98.0$

Figure 13: Example 5.6. Reference solutions of AC by IFTSRK$(11,8)$ ($\tau=0.1$, top row), large-time-step solutions of AC by pIFTSRK1$(11,8)$ ($\tau=3.5$, $\kappa=2.0$, middle row), and large-time-step solutions of pSG by pIFTSRK1$(11,8)$ ($\tau=3.5$, $\kappa=1.0$, bottom row).

$\tau=3.5$ which was larger than that allowed by IFTSRK$(11,8)$ method. We present the evolution of the maximum bounds and energy profiles obtained for the AC and pSG in Fig. 12. When there was no stabilization, as the time step increased from $\tau=0.1$ to 3.5, the solution (orange triangle curve) obtained by IFTSRK exceeded the maximum bound

($\beta=1.0$) of the AC equation, and the energy oscillated. With the introduction of $\kappa=2.0$, pIFTSRK1(11,8) stabilized the simulation, and the obtained energy profile (blue square curve) closely followed the reference profile ($\tau=0.1$). When solving the pSG equation, pIFTSRK1(11,8) with $\tau=3.5$ and $\kappa=1.0$ preserved the maximum principle and gave a very similar energy curve as the AC equation.

Fig. 13 shows the reference solutions (IFTSRK(11,8), τ=0.1) of AC, and the large-time-step solutions (pIFTSRK1(11,8), $\tau=3.5$) of AC and pSG. The annihilation of the circles occurred gradually, and the large-time-step solutions computed by pIFTSRK1(11,8) for AC and pSG were in good agreement with the reference. This demonstrates the striking similarity between pSG and AC.

Example 5.7. Finally, we considered the 3D RSLM formulation with a uniformly random distributed phase field as the initial condition

$$u(x,y,z,t=0)=1.8\times\text{rand}(x,y,z)-0.9,\quad (x,y,z)\in(-0.5,0.5)^3,$$

where rand(x,y,z) is normally distributed in $[0,1]$.

We chose $N=128^3$ and $\epsilon=0.01$. The 3D isosurfaces computed by eighth-order temporal integrators incorporated with the FD spatial discretization at $t=0,32,160$ and 360 are presented in Fig. 14. Fig. 15 shows the evolution of $\|\boldsymbol{u}\|_{l^\infty}$, absolute mass error $|M_h^n-M_h^0|$, and discrete energy E_h. It can be seen that the solution computed with $\tau=8.0$ using IFTSRK(11,8) violated the maximum-principle, and the energy curve oscillated. In contrast, the pIFTSRK1(11,8) scheme with $\tau=8.0,\kappa=1.0$ well preserved the maximum-principle and mass conservation law, and the energy decreased all the time.

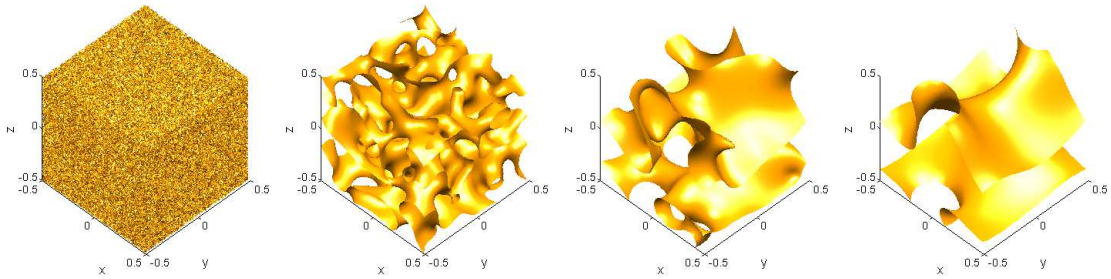

(a) $t=0$ (b) $t=32$ (c) $t=160$ (d) $t=360$

Figure 14: Example 5.7. Isosurface snapshots of solutions at $t=0,32,160,360$ computed by pIFTSRK1(11,8). Parameters: $N=128^3$, $\tau=8.0$, and $\kappa=1.0$.

6 Conclusions

In this work, a class of up to eighth-order inequality-preserving two-step integrating factor Runge-Kutta schemes were designed and analyzed to solve the pSG equation and its conservative RSLM formulation. We showed that if the underlying TSRK Butcher tableau

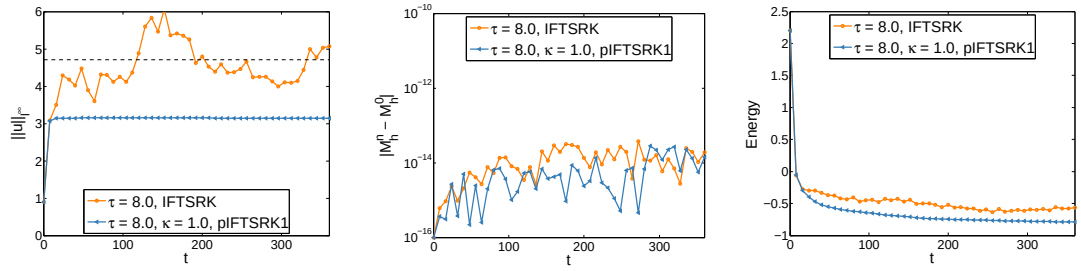

Figure 15: Example 5.7. Evolutions of $\|\boldsymbol{u}\|_{l^\infty}$ (a), absolute mass error $|M_h^n - M_h^0|$ (b), and energy E_h (c) computed by using IFTSRK$(11,8)$ $(\tau = 8.0)$ and pIFTSRK$(11,8)$ $(\tau = 8.0, \kappa = 1.0)$. The black dashed line represents level of $3\pi/2$.

has non-negative coefficients and non-decreasing abscissas, then they can be used to construct unconditionally MPP schemes. Theoretical analysis and numerical experiments demonstrated that the resulting pIFTSRK1/2 schemes with FD spatial discretization unconditionally preserve the maximum principle, and the incorporation with non-MPP FP discretization effectively improved the spatial accuracy with a negligible effect on the maximum principle. Moreover, both FD and FP discretizations conserve the mass of the RSLM formulation within machine accuracy, and numerical results indicated notable improvement of the energy stability.

Because of the particularity of the selected problems, the introduced stabilization term was of the form $\kappa(u-u)$. Thus, it is meaningful to investigate the p(IF)TSRK1/2 approaches for the mean curvature problem [12] or the Cahn-Hilliard equation [34] where a Laplacian-type stabilization $\kappa\Delta(u-u)$ is usually introduced to allow large time-step sizes. Moreover, the parametric schemes could preserve maximum principles of other problems, for example, the classical AC-type equations with either Ginzburg-Landau or Flory-Huggins potentials [19]. Appendix A also shows that the proposed schemes can preserve many other mathematical and physical inequality structures. When considering hyperbolic conservation law equations [40] or the production-destruction system [5], it is also worth researching the unconditional preservation of strong stability, positivity, or boundedness using proposed schemes.

Appendix A. Inequality-preservation of pTSRK1/2

Consider an initial value problem for a system of $N \geq 1$ ODEs of type

$$\begin{cases} \boldsymbol{u}_t = g\big(t, \boldsymbol{u}(t)\big), \quad \forall t \in (0,T], \\ \boldsymbol{u}(0) = \boldsymbol{u}^0, \end{cases} \tag{A.1}$$

where $\boldsymbol{u}^0 \in \mathbb{R}^N$, $g: \mathbb{R} \times \mathbb{R}^N \to \mathbb{R}^N$ is a continuous function. We assume that the problem (A.1) has a unique solution $\boldsymbol{u}: [0,T] \to \mathbb{R}^N$, and $\|\cdot\|: \mathbb{R}^N \to \mathbb{R}$ is a convex functional satisfying

$$\|\alpha\boldsymbol{u} + (1-\alpha)\boldsymbol{v}\| \leq \alpha\|\boldsymbol{u}\| + (1-\alpha)\|\boldsymbol{v}\|, \quad \forall \alpha \in [0,1], \quad \boldsymbol{u}, \boldsymbol{v} \in \mathbb{R}^N.$$

Let $\boldsymbol{u}^1$ be the solution at $t=\tau$ computed by a proper one-step method. We present definitions of several inequalities [4, 29, 48] relevant for the numerical stability of time integrations for (A.1).

Definition A.1 (Strong stability preservation). *A two-step method is strong stability preserving with respect to the functional $\|\cdot\|$ if*

$$\|\boldsymbol{u}^{n+1}\| \leq \max\{\|\boldsymbol{u}^n\|, \|\boldsymbol{u}^{n-1}\|\}, \quad \forall n>0$$

under the assumption that

$$\exists \tau_{FE}>0 \quad \text{such that} \quad \|\boldsymbol{u}+\tau g(t,\boldsymbol{u})\| \leq \|\boldsymbol{u}\|, \quad \forall 0<\tau\leq\tau_{FE}, \quad \forall t\in[0,T]. \tag{A.2}$$

Definition A.2 (Positivity preservation). *A two-step method is positive if, whenever $\boldsymbol{u}^j \geq 0, j=0,1$, it guarantees that $\boldsymbol{u}^{n+1}\geq 0, \forall n\geq 1$ under the assumption that*

$$\exists \tau_{FE}>0 \quad \text{such that} \quad \boldsymbol{u}+\tau g(t,\boldsymbol{u})\geq 0, \quad \forall 0<\tau\leq\tau_{FE}, \quad \forall t\in[0,T], \quad \forall \boldsymbol{u}\geq 0, \tag{A.3}$$

where the inequalities are element-wise.

Definition A.3 (Range boundedness/Maximum principle preservation). *A two-step method is range bounded in $[m,M]$ if, whenever $m\leq \boldsymbol{u}^j \leq M, j=0,1$, it guarantees that $m\leq \boldsymbol{u}^{n+1}\leq M$ under the assumption that*

$$\exists \tau_{FE}>0 \quad \text{such that} \quad m\leq \boldsymbol{u}+\tau g(t,\boldsymbol{u})\leq M, \quad \forall 0<\tau\leq\tau_{FE}, \quad \forall t\in[0,T], \quad \forall \boldsymbol{u}\in[m,M], \tag{A.4}$$

where the inequalities are element-wise. When $M=-m:=\beta>0$, the assumption (A.4) *is equivalent to*

$$\exists \tau_{FE}>0 \quad \text{such that} \quad \|\boldsymbol{u}+\tau g(t,\boldsymbol{u})\|_{l^\infty}\leq \beta, \quad \forall 0<\tau\leq\tau_{FE}, \quad \forall t\in[0,T], \quad \forall \|\boldsymbol{u}\|_{l^\infty}\leq\beta. \tag{A.5}$$

Definition A.4 (Contractivity preservation). *A two-step method is contractive if*

$$\|\boldsymbol{u}^{n+1}-\boldsymbol{v}^{n+1}\| \leq \max\{\|\boldsymbol{u}^n-\boldsymbol{v}^n\|, \|\boldsymbol{u}^{n-1}-\boldsymbol{v}^{n-1}\|\}$$

under assumption that $\exists \tau_{FE}>0$ such that

$$\|\boldsymbol{u}-\boldsymbol{v}+\tau(g(t,\boldsymbol{u})-g(t,\boldsymbol{v}))\| \leq \|\boldsymbol{u}-\boldsymbol{v}\|, \quad \forall 0<\tau\leq\tau_{FE}, \quad \forall t\in[0,T], \quad \forall \boldsymbol{u},\boldsymbol{v}\in\mathbb{R}^N. \tag{A.6}$$

By introducing $\kappa(\boldsymbol{u}-\boldsymbol{u})$ to the system (A.1), we have

$$\boldsymbol{u}_t = g(t,\boldsymbol{u})+\kappa\boldsymbol{u}-\kappa\boldsymbol{u}. \tag{A.7}$$

We show that when $\kappa\geq 1/\tau_{FE}$, pTSRK1/2 unconditionally preserve above properties when $g(t,\boldsymbol{u})$ satisfies assumptions (A.2)-(A.6) in Definitions A.1-A.4.

Theorem A.1. *For the system* (A.7) *with* $\kappa \geq 1/\tau_{FE}$*, assume underlying* TSRK *coefficients satisfy the first condition in assumption* (3.1)*, and* $g(t,\boldsymbol{u})$ *satisfies assumptions* (A.2)-(A.6) *in Definitions* A.1-A.4*. Then, solutions computed by* pTSRK1/2 *preserve properties in Definitions* A.1-A.4 *for any* $\tau > 0$*.*

Proof. Consider the preservation of contractivity in Definition A.4 using pTSRK1 as an example. Applying pTSRK1 to (A.7) with $\boldsymbol{u}^{n+j}$ and $\boldsymbol{v}^{n+j}, j=-1,0$ yields

$$\boldsymbol{u}_{n,i} = \frac{1}{\psi_i(\tau\kappa)}\left(\sum_{j=-1}^{0} d_{i,j}\mathrm{e}^{(1+c_j)\tau\kappa}\boldsymbol{u}_{n,j} + \tau\sum_{j=-1}^{i-1} a_{i,j}\mathrm{e}^{(1+c_j)\tau\kappa}\left[g(t_{n,j},\boldsymbol{u}_{n,j}) + \kappa\boldsymbol{u}_{n,j}\right]\right), \tag{A.8}$$

$i=1,\ldots,s,$

$$\boldsymbol{v}_{n,i} = \frac{1}{\psi_i(\tau\kappa)}\left(\sum_{j=-1}^{0} d_{i,j}\mathrm{e}^{(1+c_j)\tau\kappa}\boldsymbol{v}_{n,j} + \tau\sum_{j=-1}^{i-1} a_{i,j}\mathrm{e}^{(1+c_j)\tau\kappa}\left[g(t_{n,j},\boldsymbol{v}_{n,j}) + \kappa\boldsymbol{v}_{n,j}\right]\right), \tag{A.9}$$

$i=1,\ldots,s.$

Let $\kappa := 1/\tau \geq 1/\tau_{FE}$, multiplying (A.6) with κ gives the circle condition [48]

$$\|\kappa(\boldsymbol{u}-\boldsymbol{v}) + g(t,\boldsymbol{u}) - g(t,\boldsymbol{v})\| \leq \kappa\|\boldsymbol{u}-\boldsymbol{v}\|, \quad \forall \kappa \geq \frac{1}{\tau_{FE}}. \tag{A.10}$$

Subtracting (A.9) from (A.8) gives

$$\begin{aligned}\boldsymbol{u}_{n,i} - \boldsymbol{v}_{n,i} = \frac{1}{\psi_i(\tau\kappa)}\Bigg(&\sum_{j=-1}^{0} d_{i,j}\mathrm{e}^{(1+c_j)\tau\kappa}(\boldsymbol{u}_{n,j}-\boldsymbol{v}_{n,j}) \\ &+\tau\sum_{j=-1}^{i-1} a_{i,j}\mathrm{e}^{(1+c_j)\tau\kappa}\left[g(t_{n,j},\boldsymbol{u}_{n,j}) + \kappa\boldsymbol{u}_{n,j} - \left(g(t_{n,j},\boldsymbol{v}_{n,j}) + \kappa\boldsymbol{v}_{n,j}\right)\right]\Bigg),\end{aligned}$$

$i=1,\ldots,s.$ (A.11)

Taking $\|\cdot\|$ on both sides of (A.11), and applying conditions in assumption (3.1) and the circle condition (A.10) give

$$\|\boldsymbol{u}_{n,i} - \boldsymbol{v}_{n,i}\| \leq \frac{1}{\psi_i(\tau\kappa)}\left[\sum_{j=-1}^{0} d_{i,j}\mathrm{e}^{(1+c_j)\tau\kappa}\|\boldsymbol{u}_{n,j}-\boldsymbol{v}_{n,j}\| + \tau\kappa\sum_{j=-1}^{i-1} a_{i,j}\mathrm{e}^{(1+c_j)\tau\kappa}\|\boldsymbol{u}_{n,j}-\boldsymbol{v}_{n,j}\|\right],$$

$i=1,\ldots,s.$

Assuming

$$\|\boldsymbol{u}_{n,j}-\boldsymbol{v}_{n,j}\| \leq \max\left\{\|\boldsymbol{u}^n-\boldsymbol{v}^n\|, \|\boldsymbol{u}^{n-1}-\boldsymbol{v}^{n-1}\|\right\}, \quad j=1,\ldots,i-1,$$

we derive

$$\begin{aligned}\|\boldsymbol{u}_{n,i}-\boldsymbol{v}_{n,i}\| \leq \frac{1}{\psi_i(\tau\kappa)}\Bigg[&\sum_{j=-1}^{0} d_{i,j}\mathrm{e}^{(1+c_j)\tau\kappa}\max\big\{\|\boldsymbol{u}^n-\boldsymbol{v}^n\|,\|\boldsymbol{u}^{n-1}-\boldsymbol{v}^{n-1}\|\big\}\\ &+\tau\kappa\sum_{j=-1}^{i-1} a_{i,j}\mathrm{e}^{(1+c_j)\tau\kappa}\max\big\{\|\boldsymbol{u}^n-\boldsymbol{v}^n\|,\|\boldsymbol{u}^{n-1}-\boldsymbol{v}^{n-1}\|\big\}\Bigg]\\ =&\max\big\{\|\boldsymbol{u}^n-\boldsymbol{v}^n\|,\|\boldsymbol{u}^{n-1}-\boldsymbol{v}^{n-1}\|\big\},\quad i\leq s.\end{aligned}$$

By using mathematical induction, we obtain

$$\|\boldsymbol{u}^{n+1}-\boldsymbol{v}^{n+1}\|\leq\max\big\{\|\boldsymbol{u}^n-\boldsymbol{v}^n\|,\|\boldsymbol{u}^{n-1}-\boldsymbol{v}^{n-1}\|\big\}.$$

The proofs for preservations of other properties in Definitions A.1-A.3 can be performed similarly. □

Appendix B. Inequality-preserving ETD and parametric integrating factor Runge-Kutta schemes

Let $g_\kappa(t,\boldsymbol{u})=g(t,\boldsymbol{u})+\kappa\boldsymbol{u}$, the stabilization ETD2 scheme [18] for Eq. (A.1) has the form

$$\begin{cases}\boldsymbol{u}_{n,0}=\boldsymbol{u}^n,\\ \boldsymbol{u}_{n,1}=\varphi_0(-\tau\kappa)\boldsymbol{u}^n+\tau\varphi_1(-\tau\kappa)g_\kappa(t_{n,0},\boldsymbol{u}_{n,0}),\\ \boldsymbol{u}_{n,2}=\varphi_0(-\tau\kappa)\boldsymbol{u}^n+\tau\big[\varphi_1(-\tau\kappa)-\varphi_2(-\tau\kappa)\big]g_\kappa(t_{n,0},\boldsymbol{u}_{n,0})\\ \qquad\quad+\tau\varphi_2(-\tau\kappa)g_\kappa(t_{n,1},\boldsymbol{u}_{n,1}),\end{cases}\tag{B.1}$$

where the functions $\varphi_k(z)$ are recurrently defined by

$$\varphi_k(z)=\frac{\varphi_{k-1}(z)-1/(k-1)!}{z},\quad\forall k\geq 1,\quad\text{with}\quad\varphi_0(z)=\mathrm{e}^z.$$

The second type s-stage, p-th order parametric Runge-Kutta (pRK2) scheme [77] for Eq. (A.1) has the form

$$\boldsymbol{u}_{n,i}=\frac{1}{\psi_i(\tau\kappa)}\left[\boldsymbol{u}^n+\tau\sum_{j=0}^{i-1}a_{i,j}\mathrm{e}^{c_j\tau\kappa}g_\kappa(t_{n,j},\boldsymbol{u}_{n,j})\right],\quad i=1,\ldots,s,\tag{B.2}$$

where $\psi_i(\tau\kappa)$ are approximations to the exponential functions $\mathrm{e}^{c_i\tau\kappa}, i=1,\ldots,s$ given by

$$\psi_i(\tau\kappa):=1+\tau\kappa\sum_{j=0}^{i-1}a_{i,j}\mathrm{e}^{c_j\tau\kappa},\quad i=1,\ldots,s.$$

The pRK2(4,4) scheme is then constructed using the following Butcher tableau:

$$\begin{array}{c|ccc} \vdots & \cdots & \cdots & \cdots \\ c_i & \cdots & a_{i,j} & \cdots \\ \vdots & \cdots & \cdots & \cdots \\ \hline 1 & \cdots & a_{s,j} & \cdots \end{array} = \begin{array}{c|cccc} 0 & 0 & 0 & 0 & 0 \\ \frac{1}{2} & \frac{1}{2} & 0 & 0 & 0 \\ \frac{1}{2} & 0 & \frac{1}{2} & 0 & 0 \\ 1 & 0 & 0 & 1 & 0 \\ \hline 1 & \frac{1}{6} & \frac{1}{3} & \frac{1}{3} & \frac{1}{6} \end{array}.$$

Similarly as Theorem A.1, the inequality-preservation of ETD2 and pRK2 can be proven by assuming $\kappa \geq 1/\tau_{FE}$, therefore, we omit it.

Acknowledgements

The authors would like to thank the editor and the anonymous referees for their constructive comments and suggestions that greatly improved the quality of this research.

This work was supported by the National Natural Science Foundation of China (Grant Nos. 12271523, 11901577, 11971481, 12071481), by the Defense Science Foundation of China (Grant No. 2021-JCJQ-JJ-0538), by the National Key R&D Program of China (Grant No. SQ2020YFA0709803), by the Science and Technology Innovation Program of Hunan Province (Grant Nos. 2022RC1192, 2021RC3082), and by the Research Fund of National University of Defense Technology (Grant Nos. ZK19-37, ZZKY-JJ-21-01).

References

[1] S. M. Allen and J. W. Cahn, *A microscopic theory for antiphase boundary motion and its application to antiphase domain coarsening*, Acta metallurgica, 27:1085–1095, 1979.

[2] M. Bassenne, L. Fu, and A. Mani, *Time-accurate and highly-stable explicit operators for stiff differential equations*, J. Comput. Phys., 424:109847, 2021.

[3] S. Blanes, A. Iserles, and S. Macnamara, *Positivity-preserving methods for ordinary differential equations*, ESAIM Math. Model. Numer. Anal., 56:1843–1870, 2022.

[4] L. Bonaventura and A. Della Rocca, *Unconditionally strong stability preserving extensions of the TR-BDF2 method*, J. Sci. Comput., 70:859–895, 2017.

[5] H. Burchard, E. Deleersnijder, and A. Meister, *A high-order conservative Patankar-type discretisation for stiff systems of production-destruction equations*, Appl. Numer. Math., 47:1–30, 2003.

[6] M. Calvo, J. I. Montijano, and L. Rández, *A note on the stability of time-accurate and highly-stable explicit operators for stiff differential equations*, J. Comput. Phys., 436:110316, 2021.

[7] A. Chandra, M. Hairer, and H. Shen, *The dynamical sine-Gordon model in the full subcritical regime*, arXiv:1808.02594, 2018.

[8] C. Chen, T. Dang, and J. Hong, *An adaptive time-stepping full discretization for stochastic Allen-Cahn equation*, arXiv:2108.01909, 2021.

[9] L. Q. Chen and J. Shen, *Applications of semi-implicit Fourier-spectral method to phase field equations*, Comput. Phys. Commun., 108:147–158, 1998.

[10] J. Cheng and C.-W. Shu, *Positivity-preserving Lagrangian scheme for multi-material compressible flow*, J. Comput. Phys., 257:143–168, 2014.

[11] X. Cheng, D.Li, C. Quan, and W. Yang, *On a parabolic Sine-Gordon model*, Numer. Math. Theor. Meth. Appl., 14:1068–1084, 2021.
[12] K. Chow and S. J. Ruuth, *Linearly stabilized schemes for the time integration of stiff nonlinear PDEs*, J. Sci. Comput., 87:1–29, 2021.
[13] J. M. Church, Z. Guo, P. K. Jimack, A. Madzvamuse, K. Promislow, B. Wetton, S. M. Wise, and F. Yang, *High accuracy benchmark problems for Allen-Cahn and Cahn-Hilliard dynamics*, Commun. Comput. Phys., 26:947–972, 2019.
[14] S. M. Cox and P. C. Matthews, *Exponential time differencing for stiff systems*, J. Comput. Phys., 176:430–455, 2002.
[15] J. Douglas Jr. and T. Dupont, *Alternating-direction Galerkin methods on rectangles*, Numerical Solution of Partial Differential Equations-II, Academic Press, 133–214, 1971.
[16] J. Du, E. Chung, and Y. Yang, *Maximum-principle-preserving local discontinuous Galerkin methods for Allen-Cahn equations*, Commun. Appl. Math. Comput., 4(1):353-379, 2022.
[17] J. Du and Y. Yang, *Third-order conservative sign-preserving and steady-state-preserving time integrations and applications in stiff multispecies and multireaction detonations*, J. Comput. Phys., 395:489–510, 2019.
[18] Q. Du, L. Ju, X. Li, and Z. Qiao, *Maximum principle preserving exponential time differencing schemes for the nonlocal Allen-Cahn equation*, SIAM J. Numer. Anal., 57:875–898, 2019.
[19] Q. Du, L. Ju, X. Li, and Z. Qiao, *Maximum bound principles for a class of semilinear parabolic equations and exponential time-differencing schemes*, SIAM Rev., 63:317–359, 2021.
[20] Q. Du, L. Ju, and J. Lu, *Analysis of fully discrete approximations for dissipative systems and application to time-dependent nonlocal diffusion problems*, J. Sci. Comput., 78:1438–1466, 2019.
[21] Q. Du and W. Zhu, *Analysis and applications of the exponential time differencing schemes and their contour integration modifications*, BIT Numer. Math., 45:307–328, 2005.
[22] D. J. Eyre, *An unconditionally stable one-step scheme for gradient systems*, Unpublished article, 1998.
[23] J. Frenkel and T. Kontorova, *On the theory of plastic deformation and twinning*, Izv. Akademii Nauk. SSSR, Ser. Fiz., 1:137–149, 1939.
[24] Y. Gong, Q. Hong, and Q. Wang, *Supplementary variable method for thermodynamically consistent partial differential equations*, Comput. Methods Appl. Mech. Eng., 381:113746, 2021.
[25] Y. Gong, Q. Wang, Y. Wang, and J. Cai, *A conservative Fourier pseudo-spectral method for the nonlinear Schrödinger equation*, J. Comput. Phys., 328:354–370, 2017.
[26] Y. Gong, J. Zhao, and Q. Wang, *Arbitrarily high-order linear energy stable schemes for gradient flow models*, J. Comput. Phys., 419:109610, 2020.
[27] S. Gottlieb, Z. Grant, and L. Isherwood, *Optimized strong stability preserving integrating factor two-step Runge-Kutta methods*, `https://github.com/SSPmethods/ SSPIF-TSRK-methods`.
[28] S. Gottlieb, Z. J. Grant, J. Hu, and R. Shu, *High order unconditionally strong stability preserving multi-derivative implicit and IMEX Runge-Kutta methods with asymptotic preserving properties*, arXiv:2102.11939, 2021.
[29] S. Gottlieb, D. I. Ketcheson, and C.-W. Shu, *Strong Stability Preserving Runge-Kutta and Multistep Time Discretizations*, World Scientific, 2011.
[30] S. Gottlieb, C.-W. Shu, and E. Tadmor, *Strong stability-preserving high-order time discretization methods*, SIAM Rev., 43:89–112, 2001.
[31] M. Hairer and H. Shen, *The dynamical sine-Gordon model*, Comm. Math. Phys., 341:933–989, 2016.
[32] S. Ham, Y. Hwang, S. Kwak, and J. Kim, *Unconditionally stable second-order accurate scheme for a parabolic sine-Gordon equation*, AIP Adv., 12:025203, 2022.

[33] D. He, K. Pan, and H. Hu, *A spatial fourth-order maximum principle preserving operator splitting scheme for the multi-dimensional fractional Allen-Cahn equation*, Appl. Numer. Math., 151:44–63, 2020.
[34] Y. He, Y. Liu, and T. Tang, *On large time-stepping methods for the Cahn-Hilliard equation*, Appl. Numer. Math., 57:616–628, 2007.
[35] Q. Hong, Y. Gong, J. Zhao, and Q. Wang, *Arbitrarily high order structure-preserving algorithms for the Allen-Cahn model with a nonlocal constraint*, Appl. Numer. Math., 170:321–339, 2021.
[36] C. Huang, *Strong stability preserving hybrid methods*, Appl. Numer. Math., 59:891–904, 2009.
[37] J. Huang, T. Izgin, S. Kopecz, A. Meister, and C.-W. Shu, *On the stability of strong-stability-preserving modified Patankar Runge-Kutta schemes*, arXiv:2205.01488, 2022.
[38] J. Huang and C.-W. Shu, *Bound-preserving modified exponential Runge-Kutta discontinuous Galerkin methods for scalar hyperbolic equations with stiff source terms*, J. Comput. Phys., 361:111–135, 2018.
[39] W. Hundsdorfer and S. J. Ruuth, *On monotonicity and boundedness properties of linear multistep methods*, Math. Comp., 75:655–672, 2006.
[40] L. Isherwood, Z. J. Grant, and S. Gottlieb, *Strong stability preserving integrating factor two-step Runge-Kutta methods*, J. Sci. Comput., 81:1446–1471, 2019.
[41] T. Izgin, S. Kopecz, and A. Meister, *On the stability of unconditionally positive and linear invariants preserving time integration schemes*, arXiv:2202.11649, 2022.
[42] Z. Jackiewicz, *General Linear Methods for Ordinary Differential Equations*, John Wiley & Sons, 2009.
[43] Z. Jackiewicz and S. Tracogna, *A general class of two-step Runge-Kutta methods for ordinary differential equations*, SIAM J. Numer. Anal., 32:1390–1427, 1995.
[44] K. Jiang, L. Ju, J. Li, and X. Li, *Unconditionally stable exponential time differencing schemes for the mass-conserving Allen-Cahn equation with nonlocal and local effects*, Numer. Methods Partial Differ. Equ., 38:1636–1657, 2022.
[45] L. Ju, X. Li, and Z. Qiao, *Generalized SAV-exponential integrator schemes for Allen-Cahn type gradient flows*, SIAM J. Numer. Anal., 60:1905–1931, 2022.
[46] D. I. Ketcheson, *Step sizes for strong stability preservation with downwind-biased operators*, SIAM J. Numer. Anal., 49:1649–1660, 2011.
[47] D. I. Ketcheson, S. Gottlieb, and C. B. Macdonald, *Strong stability preserving two-step Runge-Kutta methods*, SIAM J. Numer. Anal., 49:2618–2639, 2011.
[48] J. F. B. M. Kraaijevanger, *Contractivity of Runge-Kutta methods*, BIT Numer. Math., 31:482–528, 1991.
[49] J. D. Lawson, *Generalized Runge-Kutta processes for stable systems with large Lipschitz constants*, SIAM J. Numer. Anal., 4:372–380, 1967.
[50] D. Li, *Effective maximum principles for spectral methods*, Ann. Appl. Math., 37:131–290, 2021.
[51] D. Li, C. Quan, and J. Xu, *Stability and convergence of strang splitting. Part I: Scalar Allen-Cahn equation*, J. Comput. Phys., 458:111087, 2022.
[52] J. Li, L. Ju, Y. Cai, and X. Feng, *Unconditionally maximum bound principle preserving linear schemes for the conservative Allen-Cahn equation with nonlocal constraint*, J. Sci. Comput., 87:1–32, 2021.
[53] J. Li, X. Li, L. Ju, and X. Feng, *Stabilized integrating factor Runge-Kutta method and unconditional preservation of maximum bound principle*, SIAM J. Sci. Comput., 43:A1780–A1802, 2021.
[54] M. Li, F. Li, Z. Li, and L. Xu, *Maximum-principle-satisfying and positivity-preserving high order central discontinuous Galerkin methods for hyperbolic conservation laws*, SIAM J. Sci. Comput., 38:A3720–A3740, 2016.

[55] H.-L. Liao, T. Tang, and T. Zhou, *On energy stable, maximum-principle preserving, second-order BDF scheme with variable steps for the Allen-Cahn equation*, SIAM J. Numer. Anal., 58:2294–2314, 2020.
[56] B. Neudecker, *Critical dynamics of the sine-Gordon model in $d=2-\varepsilon$ dimensions*, Zeitschrift für Physik B Condensed Matter, 52:145–149, 1983.
[57] M. Okumura, *A stable and structure-preserving scheme for a non-local Allen-Cahn equation*, Jpn. J. Ind. Appl. Math., 35:1245–1281, 2018.
[58] J. Rubinstein and P. Sternberg, *Nonlocal reaction-diffusion equations and nucleation*, IMA J. Appl. Math., 48:249–264, 1992.
[59] J. Shen, T. Tang, and L.-L. Wang, *Spectral Methods: Algorithms, Analysis and Applications*, Springer, Vol. 41, 2011.
[60] J. Shen, J. Xu, and J. Yang, *A new class of efficient and robust energy stable schemes for gradient flows*, SIAM Rev., 61:474–506, 2019.
[61] J. Shen and X. Yang, *Numerical approximations of Allen-Cahn and Cahn-Hilliard equations*, Discrete Contin. Dyn. Syst., 28:1669–1691, 2010.
[62] P. Smereka, *Semi-implicit level set methods for curvature and surface diffusion motion*, J. Sci. Comput., 19:439–456, 2003.
[63] L. Tang, J. Guo, and S. Song, *Bound-preserving weighted compact nonlinear schemes for scalar conservation laws with stiff source terms*, Math. Numer. Sin., 43:241–252, 2021.
[64] T. Tang, *Spectral and High-Order Methods with Applications*, Science Press Beijing, 2006.
[65] T. Tang and J. Yang, *Implicit-explicit scheme for the Allen-Cahn equation preserves the maximum principle*, J. Comput. Math., 34:471–481, 2016.
[66] J. J. van der Vegt, Y. Xia, and Y. Xu, *Positivity preserving limiters for time-implicit higher order accurate discontinuous Galerkin discretizations*, SIAM J. Sci. Comput., 41:A2037–A2063, 2019.
[67] X. Wang, J. Kou, and J. Cai, *Stabilized energy factorization approach for Allen-Cahn equation with logarithmic Flory-Huggins potential*, J. Sci. Comput., 82:1–23, 2020.
[68] X. Wang, J. Kou, and H. Gao, *Linear energy stable and maximum principle preserving semi-implicit scheme for Allen-Cahn equation with double well potential*, Commun. Nonlinear Sci. Numer. Simul., 98:105766, 2021.
[69] C. Xu and T. Tang, *Stability analysis of large time-stepping methods for epitaxial growth models*, SIAM J. Numer. Anal., 44:1759–1779, 2006.
[70] J. Xu, Y. Li, S. Wu, and A. Bousquet, *On the stability and accuracy of partially and fully implicit schemes for phase field modeling*, Comput. Methods Appl. Mech. Engrg., 345:826–853, 2019.
[71] J. Yang, Q. Du, and W. Zhang, *Uniform l^p-bound of the Allen-Cahn equation and its numerical discretization*, Int. J. Numer. Anal. Mod., 15:213–227, 2018.
[72] R. Yang, Y. Yang, and Y. Xing, *High order sign-preserving and well-balanced exponential Runge-Kutta discontinuous Galerkin methods for the shallow water equations with friction*, J. Comput. Phys., 444:110543, 2021.
[73] X. Yang, *Linear, first and second-order, unconditionally energy stable numerical schemes for the phase field model of homopolymer blends*, J. Comput. Phys., 327:294–316, 2016.
[74] H. Zhang, *Repository to verify the order conditions of pTSRK*, `https://github.com/auser account/pTSRK`, 2022.
[75] H. Zhang, J. Yan, X. Qian, X. Chen, and S. Song, *Explicit third-order unconditionally structure-preserving schemes for conservative Allen-Cahn equations*, J. Sci. Comput., 90:1–29, 2022.
[76] H. Zhang, J. Yan, X. Qian, and S. Song, *Numerical analysis and applications of explicit high order maximum principle preserving integrating factor Runge-Kutta schemes for Allen-Cahn equation*, Appl. Numer. Math., 161:372–390, 2021.

[77] H. Zhang, J. Yan, X. Qian, and S. Song, *Up to fourth-order unconditionally structure-preserving parametric single-step methods for semilinear parabolic equations*, Comput. Methods Appl. Mech. Engrg., 393:114817, 2022.
[78] X. Zhang and C.-W. Shu, *Positivity-preserving high order finite difference WENO schemes for compressible Euler equations*, J. Comput. Phys., 231:2245–2258, 2012.